Advanced Review

Printable solar cells

Seigo Ito*

Printable solar cells attract academic and industrial interests because solar cells should be cost-effective systems and have to be fabricated by non-vacuum methods such as screen printing, doctor blading, spin coating, spray deposition, and electrochemical deposition. In order to be a cost-effective solar system, the solar cells neither include expensive (indium) and toxic materials (cadmium and mercury) nor expensive processes such as chemical vapor deposition and sputtering. Similar to printed solar cells, many types of solar cells have been investigated in the past two decades: organic, dye-sensitized solar cells, $Cu(In,Ga)(S,Se)_2$, $Cu_2ZnSn(S,Se)_4$, organic thin-film photovoltaic cells, and so on. Now, the photoenergy conversion efficiencies of printed solar cells have been improved by more than 10% with the efforts of scientists. In this review, prominent progress has been presented for the future of our society.

How to cite this article:
WIREs Energy Environ 2015, 4:51–73. doi: 10.1002/wene.112

INTRODUCTION

In place of fossil and nuclear generation systems, human beings have tried to fabricate generation systems using natural energies such as hydro, biomass, geothermal, wind, and solar; of these, hydro and geothermal energies need specific areas as the mountains and hot springs, respectively. Concerning wind energy, although constant wind can be obtained from the northern sea toward Europe, the winds toward Japan and USA can be too strong (such as hurricanes, typhoons, and tornadoes), which have broken a lot of expensive wind power generations. On the contrary, solar energy can be distributed on the whole surface of the earth, which can be available to everybody, and is calm enough to be used by commercialized photovoltaic (PV) systems for decades. However, the price of the PV system was so expensive, resulting in a very high electricity price from the PV system. For example, the feed-in tariffs electricity price (Germany, at 2006) from small hydro, biogas, wind (onshore), wind (offshore), and PVs was, 6.7–9.7, 6.5–21.2, 8.4, 9.1, and 40.6–56.8 Euro cents/kWh, respectively.[1] As can be seen, the PV electricity price was four to eight times higher than that of other natural resources.

With the efforts of the PV industrial companies, the module price of PV markets went down to 57 Euro cents/Wp.[2] Because of the cheap price, however, already several PV industrial companies have been bankrupted, for example, Q-Cells (Germany), Suntech Power (China), Ever Green (USA), Solyndra (USA), Spectra Watt (USA), and so on. Therefore, the present price of PV modules is not beneficial for the healthy business of PV makers. On the other hand, the price of electricity from the PV module is still higher than the electricity fee on the grid. The target price of the PV module should be set for our future progress. The final goal was inspected as less than 50 JPY/W(module) by the Japanese government.[3] Now, one company in the USA (TetraSun) sets the target price of polycrystal silicon solar cells to be 18.5 USD cent/W(cell),[4] which can be a cost-effective solar module of 40 USD cent/W(module). This target can be the common target for every solar cell (c-Si, a-Si, CIGS, organic, and so on). Such kinds of targets will be very important to create a future sustainable society. In the review below, printable solar cells can realize the target because of the inexpensive processing cost and high-speed processing.

*Correspondence to: itou@eng.u-hyogo.ac.jp
Department of Electrical Engineering and Computer Sciences, University of Hyogo, Himeji, Japan
Conflict of interest: The author has declared no conflicts of interest for this article.

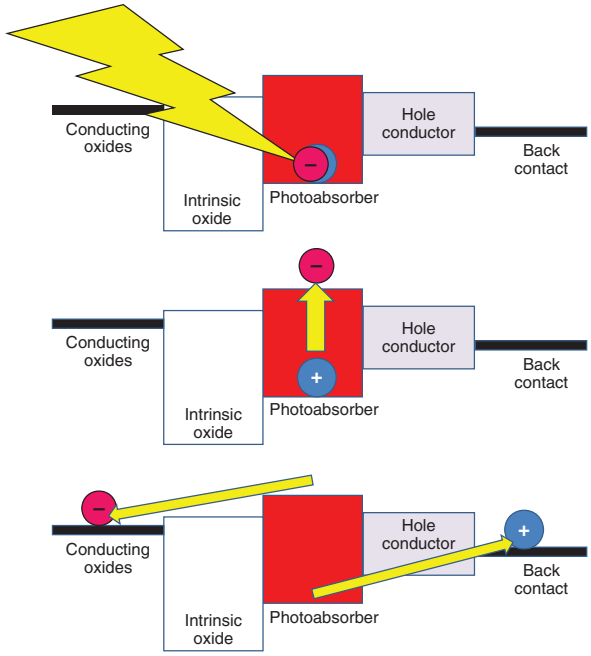

FIGURE 1 | The photovoltaic initial scheme in printed solar cells: (a) light absorption by photoabsorber; (b) electron excitation in the photoabsorber; and (c) charge separation to conducting oxide and back contact.

PRINTED SOLAR CELLS

There are three points in order to reduce the cost of solar cell fabrication, as below:

1. To omit expensive materials (In, Ag, etc.)
2. To create a simple production line without vacuum processing
3. To omit toxic materials (H_2Se, H_2S, Cd, etc.)

For the fabrication of such cost-effective solar cells, printed solar cells (by non-vacuum processing) have been investigated. In order to be a cost-effective solar system, the solar cells neither include expensive (indium) and toxic materials (cadmium and mercury) nor expensive processes such as chemical vapor deposition and sputtering. For the fabrication of printed solar cells, selection and arrangement of materials are very important. The basic sequence of PV materials is shown in Figure 1.

Each material in Figure 1 can be separate research topics. About the conducting oxides, several materials have been utilized, such as F-doped SnO_2 (FTO), Sn-doped In_2O_3 (ITO), and Al-doped ZnO (AZO). The requirements are thermal stability, chemical stability, high conductivity, and high light transmittance. About the intrinsic oxides for insulation between the conduction oxide and the photoabsorber, TiO_2, ZnO, Nb_2O_5, Y_2O_3, and most of the photocatalyst can work for the intrinsic oxide layers. The requirements are thermal stability, chemical stability, high resistibility, and the high transportation of injected electrons. About the photoabsorbers, dyes and compounds have been utilized. If we use dyes adsorbed on porous TiO_2 electrodes, they are called as dye-sensitized solar cells (DSCs). For the dyes in DSCs, ruthenium complexes have been utilized for the photoabsorber in high-efficiency DSCs. Recently, however, metal-free organic dyes have also shown good results. For the compound photoabsorbers, many materials have been attempted, such as $Cu(In,Ga)(Se,S)_2$ (CIGS), $Cu_2ZnSn(Se,S)_4$ (CZTS), Cu_2Te, PbS, $AgInTe_2$, Sb_2S_3, Se, and $CH_3NH_3PbI_3$. The requirements are for solvent deposition to be printed solar cells and for the ability of electron injection into insulating oxides. Concerning the hole conductors, electrolytes (iodide, cobalt complex, etc.), organic materials (OMeTAD, P3HT, PEDOT, PTAA, etc.), and inorganic compounds (CuI and CuSCN) have been utilized. The requirements are solvent deposition and high hole conductivity. Finally, concerning the back contact, metals (Au, Ag, Mo, Al, etc.) and carbon paste have been utilized. Although the back metal contacts have to be deposited by vacuum deposition, the carbon paste can be deposited by the printing method. The requirement is high conductivity.

Printed solar cells are categorized into two structures: superstrate and substrate. For the 'superstrate structure' (Figure 2, left), a transparent plate (glass or plastic) should be set on the photoirradiation side, and the PV device should be fabricated on the opposite side from the sun irradiation. The irradiation should pass through the transparent plate, which should be set on the top side. Then, this structure is called a 'superstrate', which has been applied to most organic printed solar cells, such as DSCs and organic thin-film photovoltaics (OPVs). The merit of this superstrate structure is that the interface between <conducting oxides/intrinsic oxides/photoabsorber> is flat, projecting the flatness of the transparent plate. Hence, the superstrate structure provides a desirable junction for the PV utilization without pin holes. The pin holes deteriorate the performance of printed solar cells owing to an internal short circuit passing through the pin holes.

On the other hand, solar cells with CIGS and CZTS have been fabricated in the 'substrate structure', which is on the opposite side from the superstrate structure (Figure 2, right). For the substrate structure, the plate is set at the bottom of the solar cells, and then, the PV device is fabricated on the plate. The top

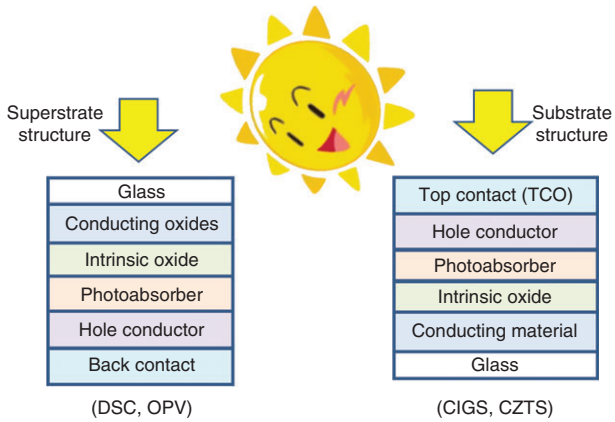

FIGURE 2 | Structure of solar cells: superstrate (left) and substrate (right) structures.

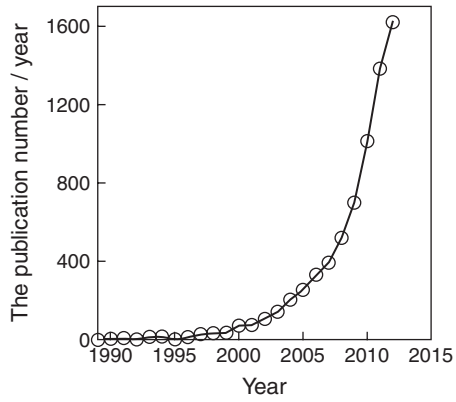

FIGURE 3 | Publication number of dye-sensitized solar cells each year from 1989 to 2012. The data were obtained by an Internet searching system (SCOPUS, ELSEVIER). The searching keywords were 'dye', 'solar', and 'cell'. The searched document type was limited only to 'article'.

of the device should be transparent conducting oxides, which can introduce the irradiated light into the photoabsorber inside. Therefore, the top surface should be quite flat or be perfectly covered by a charge-separating (oxide) thin layer. Otherwise, the PV device in substrate structure will short circuit due to the pin holes. For the high-efficiency CIGS and CZTS solar cells, the charge separation layer of CdS, $InO_xS_y(OH)_z$, or ZnO_xS_y has been coated by chemical bath deposition (CBD) on the top of the CIGS and CZTS surface. The top surface of the CIGS and CZTS layers should be very flat. Now, the EMPA group (by Prof. Tiwari) has announced the top results of CIGS solar cells (20.4% conversion efficiency) using a plastic polymer substrate with the low-temperature vacuum deposition process.[5]

In this report, major actions of non-vacuum-processed solar cells have been reviewed: DSC (liquid and solid states), compound solar cells (CIGS, CZTS, etc.), and organic thin-film solar cells.

DYE-SENSITIZED SOLAR CELLS (WITH LIQUID ELECTROLYTE)

The liquid-state DSC with a porous oxide electrode was founded by Prof. Matsumura (Osaka University, Japan).[6] The efficiency was just 1% using micron-porous ZnO electrodes for the intrinsic oxides. Later, Prof. Grätzel (EPFL, Switzerland) improved the conversion efficiency using a nanocrystalline-TiO_2 electrode adsorbed by ruthenium dye, which created the striking results of a 7% conversion efficiency.[7] After the first emersion of Grätzel-type DSCs, because of the applicable photoenergy conversion efficiency and the convenient non-vacuum high-speed printing process, thousands of papers have been published in order to push DSCs into the industrial stage

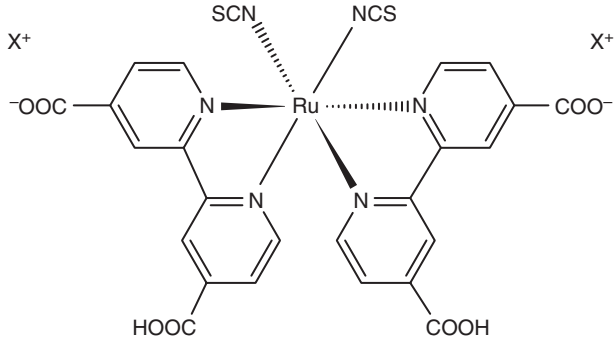

FIGURE 4 | Structures of ruthenium dyes: N3 ($X^+ = H^+$) and N719 (X^+ = tetrabutylammonium: TBA^+).[8–10]

(Figure 3). One of the key materials in DSCs is the dyes. The specially designed ruthenium-complex dyes (N3 and N719 dyes, Figure 4) have produced high-conversion efficiency liquid-state DSCs at over 10%.[8–10] Recently, 12.3% liquid-state DSCs were published using a porphyrin dye (Figure 5) by the Grätzel group.[11]

Now, the best confirmed efficiency liquid-state DSC with a liquid electrolyte is 11.4% (by NIMS, Japan), which was confirmed by AIST (Japan).[12] As an in-house measurement, the Grätzel group presented a 13% liquid-state DSC with porphyrin dye and Co-complex electrolytes.[13]

In 2009, the Miyasaka group investigated a photoabsorbing inorganic complex crystal (methylammonium lead halide: $CH_3NH_3PbX_3$, X = halogen) for the light absorber on nanocrystalline-TiO_2 electrodes as the $CH_3NH_3PbX_3$-sensitized solar cells.[14] The advantage is that the $CH_3NH_3PbX_3$ can be synthesized using simple and cheap techniques of spin coating owing to their self-assembling phenomena.

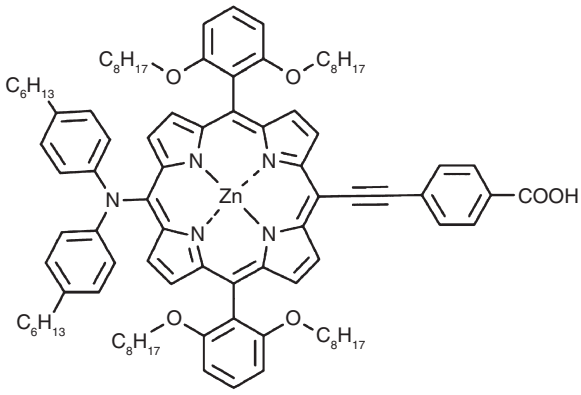

FIGURE 5 | Structures of a porphyrin dye for high-efficiency dye-sensitized solar cells (DSCs).[11]

Hence, when a solution of CH_3CH_2X and PbX_2 (X = I, Cl, or Br) was placed on a porous nano oxide layer and the layer was dried by spin coating, the $CH_3NH_3PbX_3$ solar cells could be easily fabricated. Concerning the mechanism of liquid-state DSCs, the sensitizer, adsorbed on the TiO_2 surface, absorbs a photon to produce an excited state, which efficiently transfers one electron onto the TiO_2 conduction band (CB; Figures 6 and 7). The oxidized dye is subsequently reduced by electron donation from an electrolyte containing the iodide/triiodide redox system. The injected electron flows through the semiconductor network to arrive at the back contact and passes through the external load to the counter electrode (platinum sputtered conducting glass). At the counter electrode, the reduction of triiodide in turn regenerates iodide, which completes the circuit.

The mechanism of electron transportation in porous TiO_2, called 'ambipolar diffusion', is unique.[15,16] The details of electron transportation from the dye to transparent conductive oxide (TCO) are described below (Figure 8).

1. The excited electron in the dye is injected from the dye to the TiO_2 CB (Figure 8(a,b)). At the same time, cations in electrolytes (Li^+, Na^+, K^+, TBA^+, etc.) gather to the electron-injected TiO_2 nanoparticles, and neutralize the electrical field caused by the injected electrons.
2. Before recombination between the electron in TiO_2 CB and the hole in the ground state of oxidized dye, the ground state is reduced by iodide in the electrolyte (Figure 8(c)). Because the speeds of recombination and reduction are in the order of 10^{-4} and 10^{-8} seconds, respectively, the reduction speed is faster than the recombination and the reduction can occur preferentially.
3. Electron hopping between TiO_2 nanoparticles can be performed with the assistance of charge neutralization by the gathering of cations (Figure 8(d)). Kambe et al. studied this ambipolar diffusion using several different cations (Li+, Na^+, K^+, and TBA^+) with changing concentration, and found that the speed of electron transfer varied with the kind of cation and the concentration levels.[16] Without cations in the electrolyte, no electron transfer was observed. Therefore, the assistance of the cation is necessary for the electron transfer in a nanocrystalline-TiO_2 layer. Electrons are located near the surface of TiO_2 (not inside a TiO_2 crystal).[17,18] Hence, electrons can hop from surface to surface of the nanocrystalline TiO_2. This is the reason why flexible DSCs with low-temperature annealing (<200°C) also show a high PV performance. If electrons are located inside the TiO_2 crystals, the transfer will be hindered by the nonsintered surface.
4. Breaking the charge pair between electrons in TiO_2 CB and cations in an electrolyte, the electron can hop in TCO, resulting in the current detection by the external counter (multimeter) (Figure 8(e)). In all, this electron transfer system can work effectively without a huge loss by the charge recombination between electrons and triiodides, resulting in solar cells with an efficiency of over 10%.

The explanation of the liquid-state DSC mechanism above is about the single electron transfer. In an actual case, however, excited electrons are injected into TiO_2 CB, one after another, continually. Therefore, the CB is fully occupied by the injected electrons. Würfel et al. checked the energy distribution using reference electrodes on the top of the nanocrystalline-TiO_2 layer in liquid-state DSCs.[19] In the open-circuit condition with illumination (at 720 mV), the TiO_2 CB energy level in the whole nanocrystalline-TiO_2 layer is flat (at high $V_{FTO\ vs\ Pt}$, in Figure 9), which can be explained by the negligible voltage difference between the FTO and reference Ti electrodes on the top of the nanocrystalline-TiO_2 layer [V_{int}(Ti vs FTO) at high voltage (FTO vs Pt), in Figure 10]. On the other hand, in the short-circuit condition (at 0 V), the voltage difference (between the FTO and reference Ti electrodes on the top of the nanocrystalline-TiO_2 layer) is over 600 mV (Figure 10). Hence, at the short circuit, the voltage difference between the FTO and Pt counter electrode is zero, but the voltage can drop, mainly inside the nanocrystalline-TiO_2 layer (at low $V_{FTO\ vs\ Pt}$, in Figure 9).

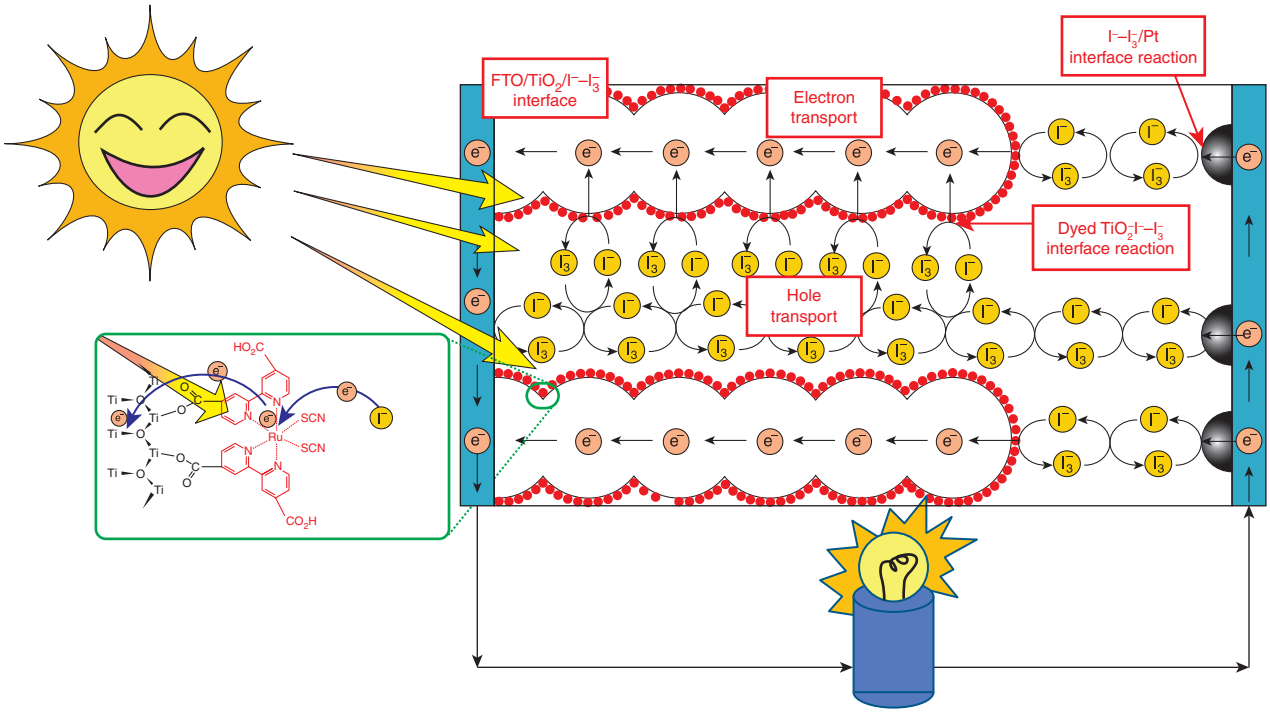

FIGURE 6 | Structure and electron movement in dye-sensitized solar cells.

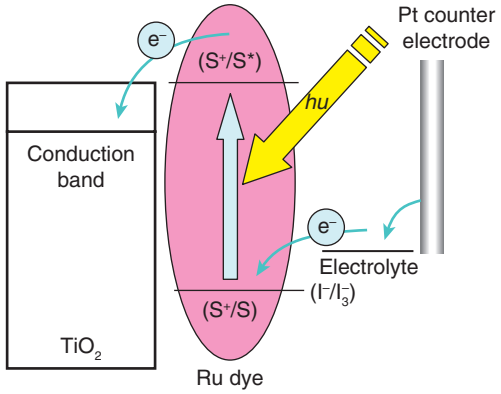

FIGURE 7 | System of electron transfer in dye-sensitized solar cells.

Although liquid-state DSCs can work effectively, the stability of solar cells has been obscure. Specifically, leakage of electrolyte and dye degradation (desorption and decomposition) have been the important issue. As cost-effective solar cells, moreover, Ru-dyes, Pt counter electrodes, and FTO-glass plates are expensive, and the photoenergy conversion efficiencies of stabilized liquid-type DSCs are less than 10%.[20] Concerning the Ru dye and the Pt counter electrodes, they can be changed to cheap organic dye and carbon electrodes, respectively. However, the durability is the difficult problem that needs to be solved because of the nature of the materials (leakage and oxidation).

Therefore, we have to think about another advantage of liquid-state DSCs other than for energy application. The unique characteristics of liquid-state DSCs are their transparency, the color from different dyes, and the beautiful design from screen-printing fabrication, which can apply to the indoor application. Now, Nissha Co. Ltd. (Japan) decided to produce liquid-state DSC with the fabrication process in 5000 cells (=12 cm submodules) per month.[21] The consistent production line from cell to module was set. The liquid-type DSC could keep the performance of a certain durability (10 years) even when it was used in outdoors. The liquid-state DSC will be commercialized as an off-grid independent power system with the beautiful design, not as an on-grid power generation. This is one of the successful examples of the liquid-state DSC application.

SOLID-STATE DSCs (WITH HOLE CONDUCTORS ON POROUS OXIDES)

Because the DSCs based on a liquid electrolyte (I^-/I_3^-) suffer from the solvent leakage and the degradation of organic constituents, solidification is a significant strategy for the application. There have been two methods to fabricate solid-stage DSCs. One is the gelation of the electrolyte, which is called 'quasi-solid DSCs'. Although the gelation prohibits the leakage of electrolytes, the vapor pressure from the volatile

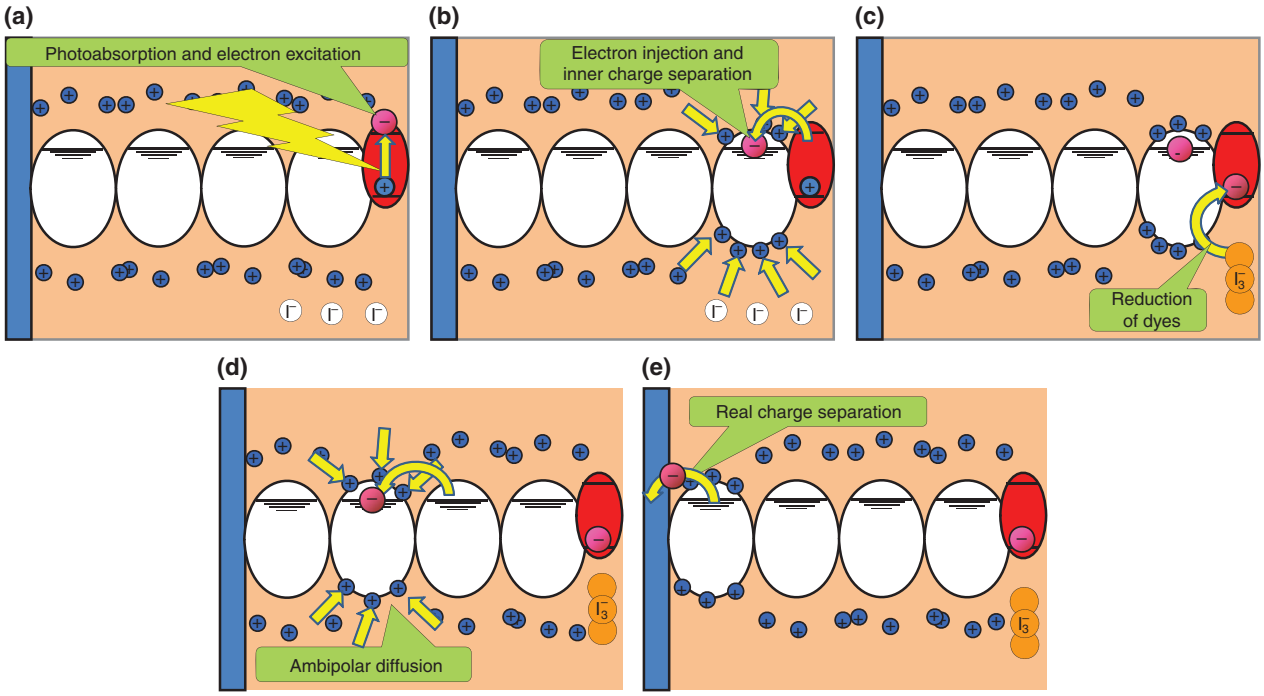

FIGURE 8 | The mechanism of electron transportation from dye to transparent conductive oxide (TCO): (a) photoabsorption and electron excitation, (b) electron injection to TiO_2 conduction band and inner charge separation, (c) dye reduction by iodide, (d) ambipolar diffusion of electron between nanocrystalline TiO_2, and (e) real charge separation of electron-cation pair.

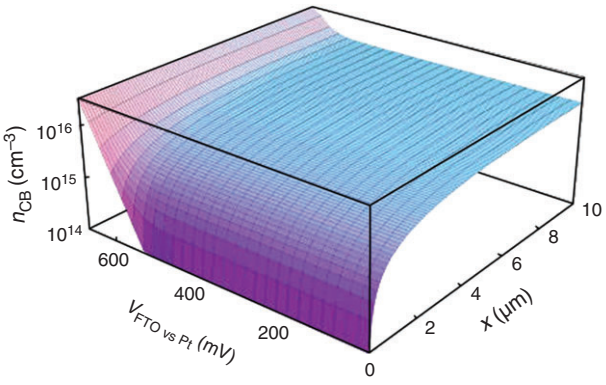

FIGURE 9 | Simulated spatial distribution of the electron concentration in the conduction band of the nanoporous TiO_2 layer (thickness d 10 μm) against the voltage applied between F-doped SnO_2 (FTO) and Pt (normal IV characteristics). It can be clearly seen that at over 500 mV there is nearly no change in the electron concentration close to the far end of the TiO_2 matrix. This is a result of the diffusion-driven current and explains the characteristics of V_{int} in Figure 10 well.[19]

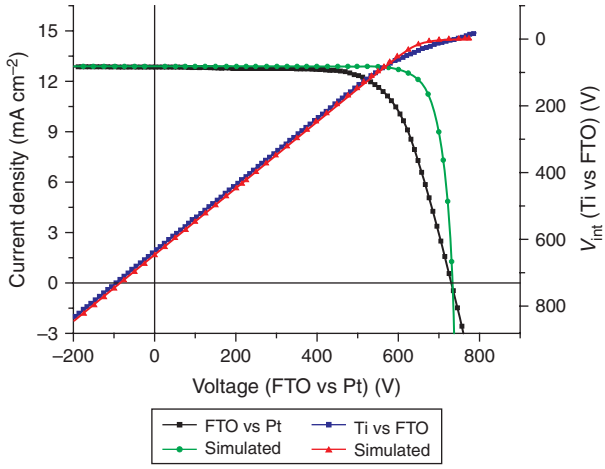

FIGURE 10 | Measured IV characteristics and simulated data of a cell with a three-electrode configuration under white light illumination equivalent to 1 sun. The normal IV characteristics between the F-doped SnO_2 (FTO) electrode and the Pt electrode (measured, black squares; simulated, green diamonds) and the internal voltage between the FTO electrode and the Ti electrode (measured, blue squares; simulated, red triangles) were sampled in parallel.[19]

solvent still can remain in DSCs. Hence, the full solidification of the electrolyte is important. Another method is the utilization of hole-conducting materials that should be introduced into the mesoporous TiO_2 by a liquid process. Hence, the hole-conducting materials have to be dissolved in some volatile solvent, to be coated in the mesoporous TiO_2, and to be solidified after the evaporation of the solvent. The base processes are spin coating or doctor blading. The variations of hole conductors have been limited to organic polymers, organic small molecules (TAD and Spiro-OMeTAD), and inorganic copper compounds

TABLE 1 | Representative Report about Solid-State Printed Solar Cells Using Small-Molecule Hole Conductors

Year	Oxides	Sensitizer	Small Molecule HTM	J_{sc} (mA/cm^2)	V_{oc} (V)	FF	Efficiency (%)	Irradiation Power (mW/cm^2)	Reference
1997	Porous TiO_2	N3	TPD	0.042	–	0.273	–	100	23
1998	Porous TiO_2	N3	Spiro-OMeTAD	0.32	0.34	0.62	0.74	9.4	24
2002	Porous TiO_2	N3	Spiro-OMeTAD	–	–	–	3.2	100	25
2005	Porous TiO_2	Z907	Spiro-OMeTAD	8.32	0.75	0.64	4.0	100	26
2005	Porous TiO_2	D149	Spiro-OMeTAD	7.7	0.87	0.61	4.1	100	27
2007	Porous TiO_2	PEG-conjugated Ru dye	Spiro-OMeTAD	11.0	0.86	0.68	5.1	100	28
2010	Porous TiO_2	Sb_2S_3	Spiro-OMeTAD	10.6	0.61	0.48	3.1	100	29
2011	Porous TiO_2	Y123	Spiro-OMeTAD + cobalt-complex dopant	9.5	0.99	0.76	7.2	100	30
2012	Porous TiO_2	$CH_3NH_3PbX_3$	Spiro-OMeTAD	17.6	0.88	0.62	9.7	100	31
2012	Flat TiO_2/porous Al_2O_3	$CH_3NH_3PbX_3$	Spiro-OMeTAD	17.8	0.98	0.63	10.9	100	32
2013	Flat TiO_2/porous Al_2O_3	$CH_3NH_3PbX_3$	Spiro-OMeTAD	18.0	1.02	0.67	12.3	100	33
2013	Porous TiO_2	$CH_3NH_3PbX_3$	Spiro-OMeTAD	20.8	0.99	0.73	15.0 (14.1, as confirmed)	100	34
2013	Flat TiO_2	$CH_3NH_3PbX_3$	Spiro-OMeTAD	21.5	1.07	0.67	15.36	100	35

FF, fill factor; TPD, triphenyldiamine; PEG, polyethylene glycol; HTM, hole transporting material; OMeTAD, 2,2',7,7'-tetrakis(*N*,*N*-diphenylamino)-9,9'-spirobifluorene; P3HT, poly(3-hexylthiophene-2,5-diyl); PEDOT, poly(3,4-ethylenedioxythiophene); PTAA, poly-tryarylamine.

(CuI and CuSCN). In some cases, the hole-conducting layer has another function as a photoabsorber, which means there are bifunctional compounds of the hole conductor and photoabsorber.

If the solid-state hole conductors have been used with an iodide source, the function of solid hole conductor can be obscure, because a very thin liquid layer with iodide in porous TiO_2 can work effectively as a hole conductor, which looks the same as solid-state devices.[22] If the solid device contained iodide anion (e.g., 1-methyl-3-propyl-imidazolium iodide: MPII) and/or was fabricated by drying a high-boiling-point solvent (e.g., *N*,*N*-dimethylformamide: b.p. 153°C), it can remain as liquid-state solar cells. It needs careful understanding to determine whether they are really solid-state solar cells or not. Hence, we should not mix such information with solid-state devices. In this section, the presentable results are shown.

Small Molecules

Although liquid-state DSCs, which have achieved efficiencies of over 10%, are interesting low-cost alternatives to conventional solar cells, solid-state DSCs had a lower performance than liquid-electrolyte DSCs until recently. However, the advantages are

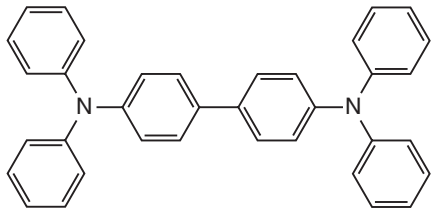

FIGURE 11 | A base structure of triphenyldiamine (TPD). The substitution group can be introduced on the side of benzine rings, depending on the purpose.

the replacement of the liquid electrolyte in these devices with a solid charge carrier material to avoid any sealing and long-term stability problems. The representative progress using small-molecule hole conductors is summarized in Table 1.

At first, the solidification of DSCs has been studied by Hagen et al. using triphenyldiamine (TPD) (Figure 11).[23] However, TPD can crystallize easily and can create an interface between the molecular crystals, resulting in the hindrance of hole hopping and in lower PV effects. Later, Spiro-OMeTAD has been investigated as an improved structure from TPD and has a high glass-transition temperature, which keeps the Spiro-OMeTAD in an amorphous phase (Figure 12).

After the investigation of spiro-OMeTAD, the major progress concerning small-molecule solid-state

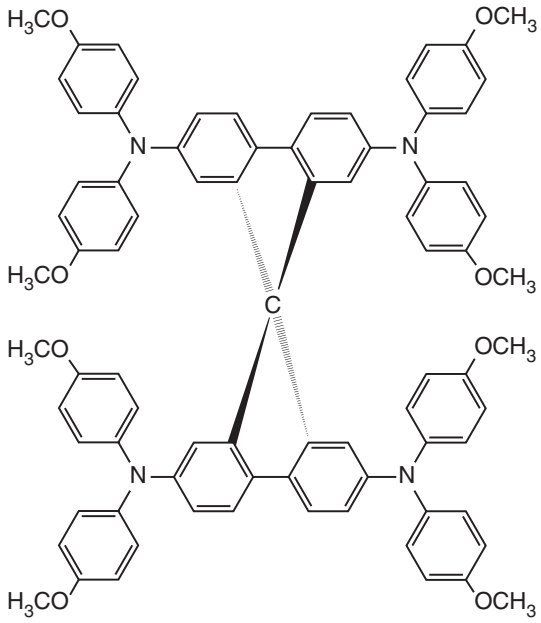

FIGURE 12 | The structure of 2,2′,7,7′-tetrakis(*N*,*N*-diphenylamino) -9,9′-spirobifluorene (Spiro-OMeTAD).

DSCs (in Table 1) has been established from the Grätzel group (or the scientists from the Grätzel group). In 1998, Bach et al. demonstrated that the electrolyte can be replaced by a hole conductor (Spiro-OMeTAD) with Ru dye (N3), which had a 0.74% conversion efficiency, as published in *Nature*.[24] Krüger et al.[25] gave the report of 3.2% efficiency by the optimization of Ru dye (N3) uptake and open-circuit voltage, which was optimized by a silver complexation. Schmidt-Mende et al.[26,27] optimized the fabrication procedures of the Spiro-OMeTAD-solid-state solar cells with ruthenium dye (Z907) or organic dye (indoline dye: D102) to a 4% conversion efficiency. Later, Snaith et al. used polyethylene glycol-conjugated ruthenium dye, resulting in over 5.1% efficiency solid-state DSCs.[28] An inorganic sensitizer (Sb_2S_3) was also utilized for the solid-state DSCs using OMeTAD to a 3.1% conversion efficiency.[29] Finally, in 2011, Burschka et al. found a significant effect on improving the efficiency by the doping of a cobalt complex up to 7.2%.[30] Since 2012, one collaboration by Park and Grätzel groups and another collaboration by Snaith and Miyasaka groups founded the combination of <porous oxides/$CH_3NH_3PbX_3$/OMeTAD>, which were excellent as solid-state solar cells. At first (in 2009), the combination of <TiO_2/$CH_3NH_3PbX_3$/I^--I_3^- electrolyte> was found by Miyasaka Lab, who had used it for liquid-state DSCs.[14] The former and latter collaborations showed 9.7 and 10.9% conversion efficiencies as the solid-state solar cells,

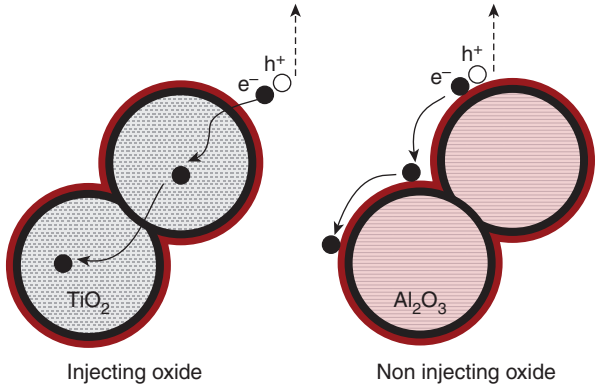

FIGURE 13 | A diagram illustrating the charge transfer and transport in a perovskite-sensitized TiO_2 solar cell (left) and a noninjecting Al_2O_3-based perovskite solar cell (right).[32]

respectively, in 2012.[31,32] Although the team of Park and Grätzel used porous TiO_2,[31] Snaith and Miyasaka used porous Al_2O_3 layers in place of porous TiO_2, which means there is a nonsensitization mechanism in the solar cells.[32] Snaith claimed that the excited electrons in the CB of $CH_3NH_3PbX_3$ can flow in the interface between Al_2O_3 and $CH_3NH_3PbX_3$ (Figure 13). However, the details are still obscure, and scientists need further experiments and discussions to understand the mechanism.

In 2013, Snaith and coworkers improved the efficiency of $CH_3NH_3PbX_3$ cells to 12.3% by optimization.[33] Very recently, the Grätzel group optimized the fabrication process of $CH_3NH_3PbX_3$ solar cells, which enhanced the conversion efficiency up to 15%, measured in-house.[34] For certified results, Newport TAC-PV Lab (USA) measured the $CH_3NH_3PbX_3$ solar cells from the Grätzel group and confirmed a 14.14% conversion efficiency.[34] Later, the Snaith group fabricated $CH_3NH_3PbX_3$ cells without a porous layer (no Al_2O_3 or TiO_2) by the vacuum deposition method to a 15.36% cell efficiency.[35] The history of solid-state $CH_3NH_3PbX_3$ solar cells is just 1 year long. The progress is on-going under high competition.

Polymers

Another idea on how to solidify DSCs is to use hole-conducting polymers such as polypyrrole and polythiophenes. The well-known representative derivatives of polythiophene are PEDOT and P3HT. The major reports are summarized in Table 2.

Considering the large size of polymer chains and the small size of the mesopore of the nanocrystalline-TiO_2 layer, the insertion of polymer materials in the mesoporous nanocrystalline-TiO_2 layer seemed quite difficult. Hagen and coworkers compared

TABLE 2 | Representative Report about Solid-State Printed Solar Cells Using Polymer Hole Conductors

Year	Porous Oxides	Sensitizer	Polymer Hole Conductors	Polymer Deposition Methods	J_{sc} (mA/cm^2)	V_{oc} (V)	FF	Efficiency (%)	Irradiation Intensity (mW/cm^2)	Reference
1997	TiO_2	N3	Polypyrrole	Electrochemical deposition	0.082	0.68	–	0.1	22	36
1999	TiO_2	N3	*p*-TPD	Spin coating	0.030	0.3	0.273	0.00246	100	37
2001	TiO_2	N3	Poly(4-undecyl-2,2′-bithiophene)	Spin coating	0.120	0.50	0.44	0.0264	100	38
2001	TiO_2	Pyrrole-conjugated Ru dye	Polypyrrole	Electrochemical deposition	0.104	0.716	0.78	0.62	10	39
2002	TiO_2	N719	P3OH	Spin coating	0.45	0.65	0.44	0.16	80	40
2004	TiO_2	N719	PEDOTs	*In situ* polymerization	2.3	0.47	0.5	0.53	100	41
2006	TiO_2	N3/PDA	P3HT	Spin coating	4.25	0.46	0.44	0.82	100	42
2006	TiO_2	Z907	Poly(3,4-ethylenedioxy-thiophene)	*In situ* photoelectrochemical polymerization	3.20	0.77	0.50	1.25	100	43
2006	TiO_2	2-Thiophen-2-yl-vinyl-conjugated Ru dye (HRS-1)	PEDOT	*In situ* photoelectrochemical polymerization	–	–	–	2.6	100	44
2008	TiO_2	P3SHT	P3SHT	Spin coating	0.980	0.438	0.33	0.142	100	45
2008	TiO_2	Z907	PEDOT	*In situ* photoelectrochemical polymerization	5.3	0.750	0.73	2.85	100	46
2010	TiO_2	D149	PEDOT	*In situ* photoelectrochemical polymerization	9.3	0.86	0.75	6.1	100	47
2010	TiO_2	Sb_2S_3	P3TH	Spin coating	12.3	0.556	0.699	5.1	94.5	48
2011	TiO_2	Sb_2S_3	PCPDTBT	Spin coating	15.3	0.62	0.66	6.2	100	49
2012	TiO_2	D35	P3HT + LiTFSI + tBP	Spin coating	6.8	0.880	0.53	3.2	100	50
2013	TiO_2	$CH_3NH_3PbX_3$	PTAA	Spin coating	19.3	0.91	0.70	12.3	100	51 52
2013	TiO_2	BzTCA/P3HT	P3HT	Spin coating	7.17	0.528	0.43	3.21	100	53

FF, fill factor; TPD, triphenyldiamine.

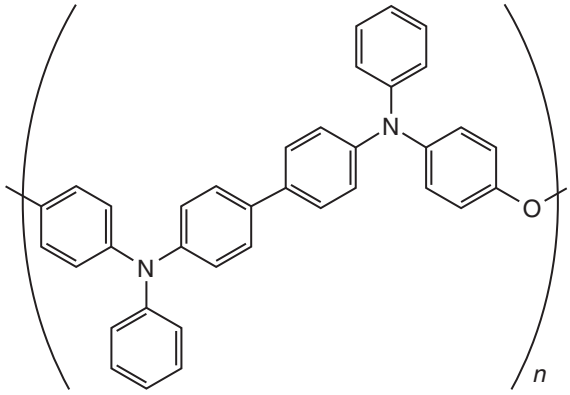

FIGURE 14 | Structure of poly-TAD.

the conversion efficiency of solid-state DSCs using small molecules (TADs) or polymers (poly-TAD) (Figure 14), showing the difficulties of polymer insertion in such mesoporous TiO_2 layers.[37] The Grätzel and Saliciftch groups tried the spin-coating method, resulting in lower PV effects.[38,40] The Yanqagia group (Osaka University, Japan) suggested the possibility of *in situ* electrochemical polymerization of polypyrrole in the dyed mesoporous TiO_2 layers.[36] Although they improved the conversion efficiencies by changing materials (ruthenium dyes and hole-conducting polymers),[39,41,43,44,46] the polymer-solid DSCs have been behind from the OMeTAD solid DSCs in the conversion efficiencies. Finally, Liu et al. found the significance of combination as <TiO_2/D149(organic dye)/PEDOT(*in situ* photoelectrochemical polymerization)> for solid-state DSCs to have a 6.1% conversion efficiency.[47]

Although spin-coating methods have shown lower efficiencies,[37,38,40,42,45] the Seok group shockingly improved the conversion efficiency by the combination of <TiO_2/Sb_2S_3/P3HT or PCPDTBT)> to a 6.2% conversion efficiency.[48,49] Using PTAA, moreover, the conversion efficiency of $CH_3NH_3PbX_3$ solid-state DSCs improved to 12.3%. The interactions between a photoabsorber (Sb_2S_3 or $CH_3NH_3PbX_3$) and hole-conducting polymers are very important to improve the PV effects.[51,52] Concerning other progress of solid-state DSCs using a polymer hole conductor by spin-coating deposition, recently, the Hagfeldt group showed a significant 3.2% conversion efficiency using organic dye (D35) with optimization of a dopant in polymers by a spin-coating method of polymer hole conductor deposition.[50] Also, Haeldermans et al.[45] and Jiang and coworkers[53] found bifunctional effects in polymers (using P3SHT and P3HT) as photoabsorber-hole conductors for solid-state DSCs to be 0.142 and 3.21% solid-state solar cells by spin-coating deposition.

Inorganic Materials

In place of organic hole conductors, inorganic hole conductors have also been investigated for the solid-state DSCs. However, in order to set the inorganic hole conductors into the porous TiO_2, the inorganic materials were dissolved into a solvent and deposited in the porous TiO_2 electrode by a liquid process. The progress is summarized in Table 3.

Since 1995, the Tennakonne group and O'Regan group have been investigating solution-processed inorganic hole conductors (CuI, CuSCN, and $4CuBr{\cdot}3SC_4H_9$).[54–67,70,74] Ruthenium dyes (N3 and N719, Figure 4) and special organic dye (D149) improved the conversion efficiency.[59,61,63–67,70,75,76] In the viewpoint of conversion efficiency, using sensitizing dye, CuI was better than CuSCN for the hole-conducting materials.

Another concept was to replace the dye with an extremely thin layer of a low-bandgap semiconductor to form the structure <porous TiO_2/low-bandgap semiconductor (extremely thin layer)/solid hole collector>. Subsequent systems of the above structure were named as extremely thin absorber (ETA) solar cells. Considering the stability for solar cell application, the inorganic hole-conducting material with the inorganic photoabsorber has attracted attention from the industry, because of the ease of fabrication of all-solid-state, fully inorganic printed solar cells. For the inorganic-sensitizing materials in solid-state ETA cells with inorganic hole conductors (CuI or CuSCN), Se,[60] CdS,[69] CdSe,[68] In_2S_3,[71] Sb_2S_3,[72–74,77] and $CH_3NH_3PbX_3$[78] have been utilized. Of these, Sb_2S_3 is especially important because of its low bandgap, band offset matching, and availability of techniques for CBD on porous TiO_2 electrodes. The CBD technique for Sb_2S_3 deposition has been reported by many authors since the early 1990s.[79,80] These thin films show a defined crystal structure of the stibnite (Sb_2S_3) of the orthorhombic system after annealing at 300°C. Crystal Sb_2S_3 with a stibnite structure has a bandgap of 1.7–1.8 eV.

To improve Sb_2S_3-ETA, all-solid-state, fully inorganic printed solar cells, it is necessary to decrease the recombination of carriers, which consists of four interfacial recombination pathways: a recombination of injected electrons in the CB of TiO_2 with either holes in the absorber or in a p-type semiconductor (CuSCN or CuI), recombination of electrons in the absorber with holes in the hole conductor, or recombination in the absorber itself. In order to increase the physical separation of injected electrons from the Sb_2S_3 or CuSCN in ETA solar cells, blocking layers (Al_2O_3) on a nanocrystalline-TiO_2 electrode have been utilized, resulting in the best Sb_2S_3 ETA

TABLE 3 | Representative Report about Solid-State Printed Solar Cells Using Inorganic Hole Conductors

Year	Porous Oxides	Sensitizer	Inorganic Hole Conductors	J_{sc} (mA/cm^2)	V_{oc} (V)	FF	η (%)	Irradiation Power (mW/cm^2)	Reference
1995	TiO_2	Cyanidin	CuI	2.5	0.375	–	0.8	80	54
1996	TiO_2	Rhodamine DHPE	CuSCN (electrodeposition)	0.038	0.550	–	–	30	55
1997	TiO_2	Copper chlorophyllin	CuI	2	0.435	–	0.7	80	56
1998	TiO_2	Ru dye (Z105)	CuSCN (electrodeposition)	0.044	0.600	–	–	100	57
1998	TiO_2	Santalin	CuSCN	2	0.500	–	–	80	58
1998	TiO_2	Santalin	CuI	6	0.450	–	1.8	80	58
1998	TiO_2	Ruthenium dye (N3)	CuI	–	–	–	4.5	100	59
1998	TiO_2	Selenium (electrochemical deposition)	CuSCN	3	0.600	–	0.13	80	60
1999	ZnO/SnO_2	Ruthenium dye (N3)	CuI	4.8	0.832	–	2.4	100	61
2000	ZnO	A ruthenium dye (Z105)	CuSCN (electrodeposition)	4.5	0.550	0.57	1.5	100	62
2000	ZnO	Ruthenium dye (N3)	4CuBr·3S(C_4H_9)	4.3	–	–	0.6	100	63
2001	TiO_2	Ruthenium dye (N3)	CuSCN	3.52	0.616	0.58	1.25	100	64
2002	TiO_2	Ruthenium dye (N3)	CuSCN	7.8	0.59	0.44	2.0	100	65
2004	TiO_2/MgO	Ruthenium dye (N3)	CuI	13.0	0.62	0.58	4.7	100	66
2005	TiO_2	Ruthenium dye (N3)	CuSCN (doping)	9.09	0.604	0.455	2.39	100	67
2005	ZnO	CdSe	CuSCN	4	0.5	–	2.3	36	68
2006	TiO_2	CdS	CuSCN	2.3	0.86	0.65	1.3	100	69
2007	TiO_2	D149	CuI	14.1	0.551	0.54	4.2	100	70
2008	ZnO (nanorod)	In_2S_3	CuSCN	10.5	0.57	0.56	3.4	100	71
2009	TiO_2	In-OH-S/Sb_2S_3	CuSCN	14.1	0.49	0.49	3.4	100	72
2010	TiO_2/Al_2O_3	Sb_2S_3	CuSCN + LiSCN dopant	11.6	0.56	0.58	3.7	100	73
2012	TiO_2/$BaTiO_3$/MgO	Sb_2S_3	CuSCN	13.4	0.58	0.53	4.1	100	74
2012	TiO_2	Ruthenium dye (N719)	CuI	12.8	0.65	0.72	6.1	100	75
2012	TiO_2	Ruthenium dye (N719)	CuSCN	10.52	0.578	0.556	3.39	100	76
2013	TiO_2	Sb_2S_3 + Ti dopant	CuSCN	15.0	0.70	0.53	5.7	100	77
2013	TiO_2	Se/$CH_3NH_3PbX_3$	CuSCN	15.4	0.67	0.57	6.0	100	78

FF, fill factor.

solar cells with a 3.7% conversion efficiency and a CuSCN hole conductor.[73]

In our group, in order to improve Sb_2S_3 ETA solar cells using nanocrystalline TiO_2 and CuSCN as the n-type porous electrode and the p-type hole collector, respectively, we have optimized the size of the nanocrystalline TiO_2, the thickness of nanocrystalline-TiO_2 electrodes, the concentration of the CuSCN solution for deposition, the thickness of the CuSCN hole-conducting layer, and the influence of the TiO_2 surface treatment in Mg^{2+}, Ba^{2+}, and Al^{3+}. Also, both Mg^{2+} and Ba^{2+} (named 'double treatment') on the PV properties were thoroughly investigated. The best cells using double treatment in Mg^{2+} and Ba^{2+} attained a short-circuit photocurrent of 13.4 mA/cm^2, an open-circuit voltage of 0.584 V,

a fill factor of 0.525, and a conversion efficiency of 4.10% at 1 sun irradiation.[74]

We have conducted further investigations into metal-element doping of the Sb_2S_3-ETA layer, and have attempted doping with several compounds: $TiCl_4$, $ZnCl_2$, and $BiCl_3$. Although Bi doping in Sb_2S_3 narrowed the Sb_2S_3 bandgap (from 1.72 to 1.59 eV), it did not shift the incident-to-photocurrent conversion efficiency (IPCE) edge or improve the photocurrent. However, doping with Ti and Zn improved the IPCE and the photocurrent. The best conversion efficiency of Sb_2S_3-ETA solar cells was 5.7% with Ti doping.[77] As the latest results, we have presented a 6.0% conversion efficiency of printed, inorganic, and sensitized solar cells with the structure of <FTO/TiO_2/Se/$CH_3NH_3PbI_3$/CuSCN/ Au>.[78] The progress is on-going.

COMPOUND SOLAR CELLS WITH BIFUNCTION OF PHOTOABSORPTION AND HOLE CONDUCTION

Compound solar cells, such as CIGS and CZTS, have received consideration from many researchers around the world because of their attractive properties: high stability and efficiency, and the diversity of fabricating methods, including both vacuum and non-vacuum methods such as coevaporation, sputtering, printing, and spin coating. The record conversion efficiencies of vacuum-deposited CIGS solar cells were 20.3% on the glass substrate with Mo as a back contact[81] and 20.4% on polymer flexible substrates[5] using cadmium sulfide as the buffer layer. Without the cadmium element, the Nakada group (Aoyama Gakuin University, Japan) fabricated 18.4% CIGS solar cell,[82] which is commercialized by Solar Frontier Co. Ltd. (Japan) as Cd-free CIGS solar cells.

As the indium element in CIGS solar cells is quite expensive, CZTS solar cells have been investigated by Prof. Katagiri as indium-free compound solar cells.[83,84] Concerning CZTS solar cells, the conversion efficiencies of 9.15%[85] and 11.1%[86] have been reported using the vacuum coevaporation method and hydrazine-based spin-coating process, respectively. The structure was mainly the 'substrate structure' (Figure 2). Basically, the component of compound solar cells contains intrinsic-oxide layers such as ZnO and TiO_2 (Figures 1 and 2). The durability and efficiency of compound solar cells are higher than those of the other printed solar cells such as polymer and DSCs. Although the conversion efficiency of non-vacuum-processed compound solar cells was lower than that of vacuum-processed compound solar cells (except for CZTS solar cells), the non-vacuum methods are quite attractive because they are a simple and high-speed process. In addition, the production setup is cost-effective. For these reasons, they are expected to be low-cost solar cells in the future. If the compound solar cells were printed in ambient air without vacuum processing and without toxic and explosive chemicals (e.g., hydrazine, KCN, H_2Se, and H_2S), they can offer a promising strategy for future research and industrial investigation into cost-effective PV systems. In this report, the fabrication methods of chemical synthesis, ball-milling synthesis, spray pyrolysis deposition (SPD), and electrochemical deposition have been reviewed.

Chemical Synthesis of Photoabsorber Compound Layers

The structures of chemically based CIGS (or CZTS) solar cells are 'substrate' (Figure 2). Todorov et al. (in IBM group) obtained a conversion efficiency of 15.2%[87] and 11.1%[86] with CIGS and CZTS solar cells fabricated by the solution process using a hydrazine solvent, respectively; however, the hydrazine is highly toxic for the mass production of PV cells. By printing CIGS and CZTS nanoparticles with several KCN etchings before annealing, Guo et al. showed a 12.0%[88] and 8.4%[89] conversion efficiency, respectively, without the hydrazine method. Our group found a significant difference in the KCN effect before and after annealing.[90] Thinking about the Guo's results, the KCN etching before annealing may remove organic materials between the $CuInS_2$ nanoparticles.[88,89] Also, the KCN etching after annealing may remove CuS_x on the top surface of $CuInS_2$ layers.[90] These CIGS (or CZTS) nanoparticles have been synthesized by the hot-injection method: the sulfur is injected into the metal-source (Cu-In-Ga or Cu-Sn-Zn) hot solution of oleylamine (at 250°C).[90] In some cases, however, the synthesis of CIGS and CGTS nanoparticles is difficult. In place of the synthesis of metal-sulfur particles, Park et al. reported that metal oxides of precursors (Cu-In-Ga) were prepared by a precursor solution-based coating method with an oxidation process, and then, the oxide layers were sulfurized by a heat treatment process to become a CIGS thin layer, resulting in the solar power conversion efficiency of 8.28% under standard irradiation conditions.[91]

Using Pb, new printable materials have been investigated, such as PbS and $CH_3NH_3PbX_3$, which are bifunctional materials such as the photoabsorber and hole conductor on nanocrystalloine-TiO_2 (or ZnO) electrodes. PbS nanoparticles were spin-coated on nanocrystalline-TiO_2 (or ZnO) electrodes,

resulting in a 4–6% conversion efficiency.[92–95] $CH_3NH_3PbX_3$ solar cells were fabricated just by the spin coating of a mixed solution of CH_3NHX and PbX_2 on nanocrystalline-TiO_2 electrodes, resulting in a 5.5% conversion efficiency.[96]

Ball-Milling Synthesis of Photoabsorber Compound Particles

For the preparation of chalcopyrite-type $CuInSe_2$, a nonheating ball-milling (mechanochemical) process has been investigated by the Wada group (Ryukoku University, Japan).[97] They prepared a fine CIGS powder suitable for screen printing using the mechanochemical process. The CIGS crystal structure was confirmed by X-ray diffraction. The CIGS solar cells with a <Al grid/B-doped ZnO/i-ZnO/CdS/CIGS/Mo/sodalime glass> 'substrate' structure (Figure 2) were fabricated, as 2.7% conversion efficiency.[98] In our group, $CuInSe_2$ powders synthesized by ball milling were printed on <In_2S_3/TiO_2/FTO/glass plates>, resulting in 'superstrate' solar cells (Figure 2) without using KCN, H_2S, or H_2Se.[99] Although the particle structure of $CuInSe_2$ in the layer remained after heating at 600°C under N_2 gas, PV effects were observed; the open-circuit voltage and short-circuit current density were 0.45 V and 5.6 mA/cm^2, respectively. On the other hand, the substrate-structure solar cells did not work at all owing to the roughness of top surface.

For another candidate of printed PV materials, Cu_2Te[100] and $AgInTe_2$[101] particles were synthesized by ball milling and then printed on <In_2S_3/TiO_2/FTO-glass plate>, resulting in superstrate-structured solar cells (Figure 2). The bandgap of the Cu_2Te and $AgInTe_2$ films was approximately 0.8 and 0.67 eV, respectively, which can work for narrow bandgap materials in tandem solar cells. The PV characteristics of the best full Cu_2Te cells were obtained by annealing at 400°C (energy conversion efficiency: 1.57%). The short-circuit photocurrent density of $AgInTe_2$ solar cells strongly increased up to 18 mA/cm^2 for the samples annealed at 600°C.

SPD Method

Concerning $CuInS_2$ solar cells by SPD, the structures are 'superstrate' (Figure 2). Goossens group[102] and Vijayakuma group[103] fabricated 7 and 9.5% conversion efficiency $CuInS_2$ solar cells, respectively. However, the reproducibility seems very difficult, because their latest publications show a lower conversion efficiency than the former published results: 2.2 and 2.13% from the Goossens and Vijayakumar groups, respectively.[104,105] In our group, flat-CIS solar cells and three-dimensional (3D) compound solar cells have been fabricated on <FTO/flat-TiO_2/In_2S_3/$CuInS_2$/Au> and <FTO/compact TiO_2/porous TiO_2/$In_x(OH)_ySz$/$CuInS_2$/Au> with 1.7 and 3.2% conversion efficiencies, respectively.[106,107]

Basically, spray-deposited CIS solar cells have been fabricated on a TiO_2 layer. We have fabricated CIS solar cells with a superstrate structure on flat-ZnO layers, which were fabricated from zinc chloride, and zinc acetylacetonate precursors had a rougher surface than film fabricated from the zinc acetate dehydrate precursor. The parameters of the best cells were a short-circuit photocurrent density of 9.72 mA/cm^2, open-circuit voltage of 0.55 V, fill factor of 0.45, and efficiency of 2.50%.[108] On the contrary, <FTO/ZnO rod/In_2S_3/$CuInS_2$> type ETA cells were prepared by an in-line chemical spray pyrolysis method. The effects of buffer layer thickness and ZnO nanorod length (500–1000 nm) were studied. The highest conversion efficiency of 4.17% at AM1.5 was recorded from a small contact area of the cell based on rods with a length of 600 nm.[109]

Concerning sprayed $CuInS_2$ films, we found a significant difference of images between the scanning electron microscope and optical microscope, which suggests segregation of spray pyrolysis $CuInS_2$ particles in the In_2S_3 layer.[110] Moreover, transmission electron microscopy/energy-dispersive X-ray (TEM-EDX) analysis revealed significant differences of the atomic ratio in the spray-deposition layer, which suggested the strong segregation of the Cu-In-S elements in the spray pyrolysis-deposited layer.[111]

Concerning spray pyrolysis CZTS solar cells, the reported conversion efficiencies were around 2%.[112,113] In place of CZTS materials, Cu-Zn-S (CZS) films, which were omitted by the Sn element, were deposited by the spray pyrolysis method. The as-deposited CZS film showed a low crystallinity. The resistivity of the CZS film with a Cu/(Cu + Zn) ratio of 50% is around 10^{-2} Ω cm. The CZS film elements using the spray Cu–Zn (=1:1) solution with thiourea was confirmed as Cu:Zn:Sn = 2:2:3 by ICP-MS and EDX. The bandgap of CZS films varied in the range of 1.8–3.5 eV when the Cu/(Cu + Zn) ratio was increased from 0 to 67%; the CZS film with a Cu/(Cu + Zn) ratio of 50% showed a wide bandgap of 2 eV. The PV characteristics were confirmed as having a cell structure of <glass/FTO/TiO_2/In_2S_3/CZS/carbon>. The best cell was observed in the CZS films with a Cu/(Cu + Zn) ratio of 50%; these cells depicted a conversion efficiency of 1.7%.[114]

For spray pyrolysis CIS solar cells, different back contact electrodes of Al, Cu, Mo, Au, and C (carbon)

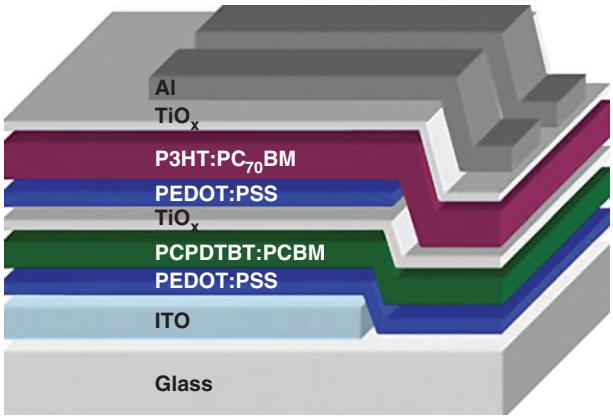

FIGURE 15 | Structure of tandem cell by Heeger et al. [$J_{SC} = 7.8$ mA/cm^2, $V_{OC} = 1.24$ V, fill factor (FF) = 0.67, and $\eta = 6.5\%$].[128]

have been adopted. Although the conversion efficiency of the cells using Al and Cu back contacts significantly deteriorated after 1 month of keeping devices in air ambience, the device performance of the CIS cells using Au, Mo, and carbon was quite stable after 1 month. The resulting CIS solar cells, fabricated by SPDs for CIS layers and screen printings for carbon layers, are recognized as full non-vacuum fabricated solar cells.[115]

Electrochemical Deposition

Stacked metal layers (In, Ga, and Cu) were prepared by electrochemical deposition to form precursor films. Thermal annealing treatments in the presence of a chalcogen (selenium or sulfur) over pressure can improve CIGS or $CuInS_2$ layers for solar cells. The Lincot group and Matsumura group performed 11.3 and 7.8% conversion efficiencies of electrochemical-deposited CIGSe and CIS solar cells, respectively.[116,117] In contrast, a one-step electrochemical deposition of a Cu-In-Ga mixed oxide precursor film on an Mo substrate is carried out by a potentiostatic method in an acidic nitrate-based electrolyte. The oxide layer is subsequently transformed into a metallic alloy by thermal reduction, and selenized into a CIGS compound. The first cell results show a conversion efficiency of up to 9.4%.[118]

Electrochemical-deposited Cu_2ZnSnS_4 and $Cu_2ZnSnSe_4$ solar cells have also progressed. Pawar et al. fabricated CZTS solar cells with 1.21% by the one-step electrodeposition technique followed by H_2S annealing.[119] The Scragg group and Schock group fabricated Cu_2ZnSnS_4 solar cells with a 3.2 and 3.4% conversion efficiency by sequential electrodeposition of a metal precursor followed by annealing in sulfur or an H_2S atmosphere, respectively.[120,121] High-performance $Cu_2ZnSnSe_4$ PV materials were synthesized by electrodeposition of metal stack precursors followed by selenization (7.0% efficiency).[122]

In place of CIGS and CZTS materials, we tried to fabricate a 3D selenium solar cell by an electrochemical deposition method. The structure was <fluorine-doped tin oxide-coated glass plates/compact TiO_2/porous TiO_2/selenium/Au>. The selenium can function for the extremely thin light absorber and the hole-conducting layer at the same time. The cells with a selenium layer deposited at concentrations of HCl = 11.5 mM and H_2SeO_3 = 20 mM showed the best performance, resulting in a 1- to 2-nm thickness of the Se layer, a short-circuit photocurrent density of 8.7 mA/cm^2, an open-circuit voltage of 0.65 V, a fill factor of 0.53, and a conversion efficiency of 3.0%.[123]

ORGANIC THIN-FILM SOLAR CELLS

At first, Tang (Kodak Company, USA) fabricated organic p-n junction thin-film solar cells using perylene and Cu phthalocyanine by the vacuum deposition method, resulting in a 1% conversion efficiency in 1986.[124] Later, much effort has been applied on the research topic. Hiramoto et al. fabricated bulk heterojunction organic thin-film solar cells by coevaporations.[125] Sariciftci et al. found the significant effects of fullerene (C_{60}) on the organic thin-film solar cells.[126] Later, phenyl C_{61}-butyric acid methyl ester (PCBM) was investigated as a solvent-soluble molecule (fullerene cannot dissolve into a normal organic solvent), which can become the printed solar cells. At first, bulk heterojunction OPVs using poly(2-methoxy-5-(2′-ethyl-hexyloxy)-1,4-phenylene vinylene) (MEH-PPV) and PCBM have been fabricated by Heeger and coworkers, resulting in 1.5% conversion efficiencies.[127] In order to improve the conversion efficiency further, tandem structure was performed, resulting in a 6.5% conversion efficiency (Figure 15), in which TiO_2 charge separation layers have been utilized, as in Figures 1 and 2.[128] Now, the best single-junction and tandem-structure OPVs published have 9.2 and 10.6% conversion efficiencies, respectively.[129,130] From the companies Mitsubishi chemicals Co. Ltd. (Japan) and Helitek GmbH (Germany), organic thin-film solar cells were fabricated with 11.7 and 12.0% conversion efficiencies, respectively (announced on their homepage).

However, these solar cells were not stable against water and oxygen, which needed an O_2-purged glove box and very rigid sealing to block the leakage of water and oxygen. A lot of progress was made by the Takahashi group (Kanazawa University,

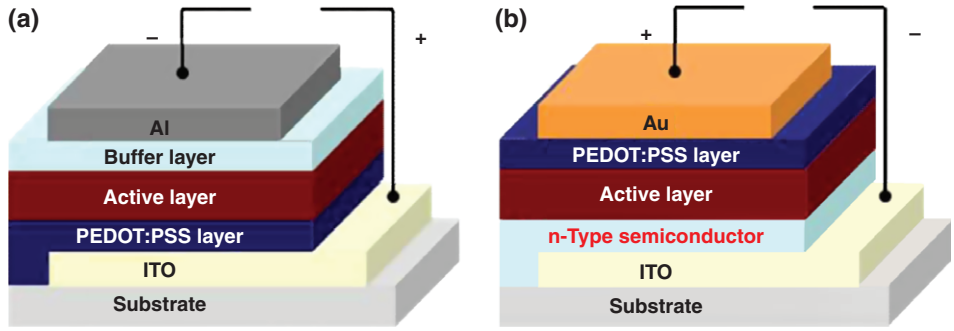

FIGURE 16 | Schematic structures of normal (a) and inverted-type organic solar cells (b).[131]

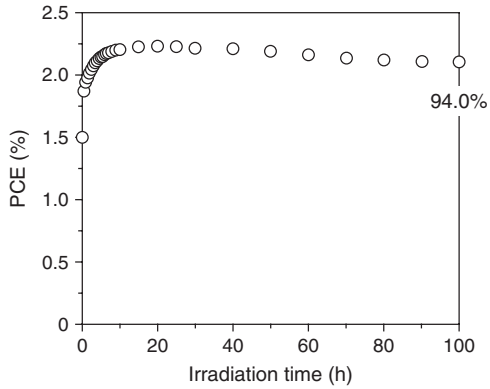

FIGURE 17 | Irradiation time dependence of the photocurrent conversion efficiency (PCE) for the nonsealed CBDTiOx-inserted cell in air. The PCBM:P3HT blend film was prepared using the CB solution. The PCE maintained 94.0% of the maximum value (2.23%) even after continuous light irradiation for 100 h.[131]

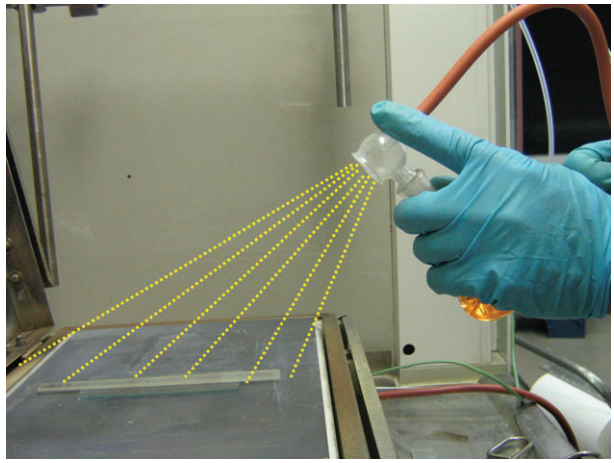

FIGURE 18 | Photograph of spray pyrolysis deposition of dense TiO_2 layer.

Japan) concerning this matter. They made inverted bulk heterojunction organic thin-film solar cells with TiO_2 layers (Figure 16), which can survive without encapsulation (Figure 17).[131] Currently, further progress is being made.

PRINTING METHODOLOGIES FOR SOLAR CELLS

Finally, in this chapter, typical printing methods for printable solar cell are summarized. In this article, the meaning of printing was extended to non-vacuum methods. Therefore, the methods for printed solar cells are SPD, screen printing, doctor blading, spin coating, CBD, self-assembling monolayer (SAM), and electrochemical deposition (electrodeposition and plating). Each method needs its own ink composition and equipment. In order to explain the methods, these are categorized into four types: (1) SPD, (2) ink deposition, (3) soaking method, and (4) electrochemical deposition.

(1) *Spray pyrolysis deposition* (SPD)

For this method, the materials for the targeting layer were dissolved in the solvent (water, ethanol, etc.), sprayed onto the hot substrate at 200–600°C, and reacted to the aimed layer (Figure 18). For example, in order to obtain a dense TiO_2 layer by the SPD method, diisopropoxy titanium acetylacetonate in ethanol was sprayed onto the substrate at 450°C. The thickness was controlled by changing the deposition volume of the solution.

(2) *Methods of ink deposition (screen printing, doctor blading, and spin coating)*

These methods need source ink for printable solar cells. Basically, the ink contains nanoparticles of solar cell materials (TiO_2, CIGS, CZTS, etc.). In order to print the ink on the targeting substrate homogeneously, the ink should contain an organic surfactant. The combination of the surfactant and solvent can change the viscosity, which decides the method of coating of either screen printing, doctor blading, or spin coating. For the high-viscous (solid) paste, the screen printing method is utilized, which is performed with a screen mesh and a stage to hold the mesh (Figure 19). For the low-viscosity (liquid) paste,

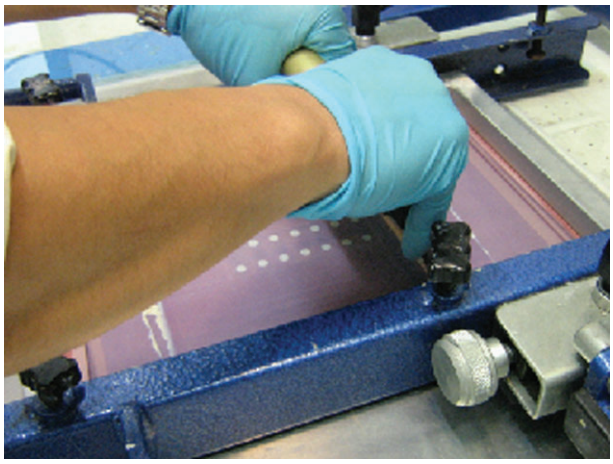

FIGURE 19 | Photograph of screen printing for porous TiO_2 layer.

FIGURE 20 | Photograph of spin coating.

the spin-coating method is applied, which needs a spin coater (Figure 20). The doctor blading method is applied on a wide range of paste viscosity and only needs adhesive tape for the laboratory trial (Figure 21). The adhesive tape is used for the spacer between the glass rod and the substrate to print the ink. The thickness of the layer is decided by the thickness of the adhesive tape.

(3) *Soaking methods (CBD and SAM)*

Contrary to the ink deposition methods, CBD and SAM are deposition methods by chemical reactions, which can give a conformal layer on a rough surface. For these methods, the tools are just bottles and substrates. Sometimes, it is important to control the deposition temperature.

The CBD method is used for crystal growth of an inorganic semiconductor layer and can control the thickness and structure of crystals by changing the bath conditions (pH, temperature, surfactant, solvent, cation, and so on). The available crystals are oxides,

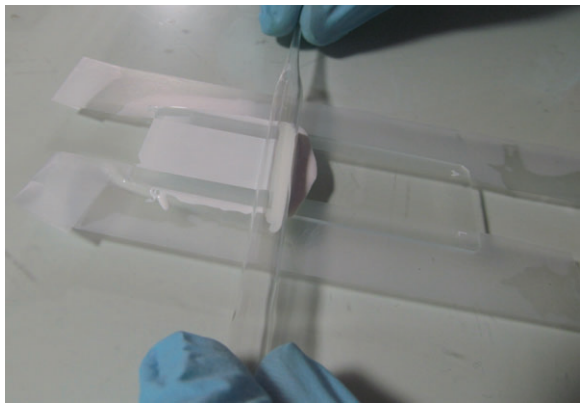

FIGURE 21 | Photograph of doctor blading of TiO_2 paste.

sulfides, and selenides. The inorganic semiconductor layers by CBD can be used for buffer layers in CIGS and CZTS solar cells, ETA layer, and nanocrystalline structure oxides. The nucleation of crystal growth can occur not only on the substrate surface but also in the solution (Figure 22). The controlling of nucleation requires the knowledge of materials.

The SAM needs the reaction between the surface of the substrate and molecules in a solution, resulting in the monolayer on a substrate. Carboxylic acid and phosphoric acid can react and be anchored to the surface of metal oxides. On the other hand, the thiol group can react and be anchored onto metals. This technique has been used for dye up-taking for DSCs.

(4) *Electrochemical deposition (electrodeposition and plating)*

In order to fabricate the electrochemical-deposited layers, electrochemical equipment is used (basically potentiostat). The latest system has been controlled by PC software, which can apply the constant voltage and the pulsed voltage. Using a reference electrode, the targeting voltage can be applied on the working electrode from the equilibrium cell voltage. For the porous substrate, the pulsed voltage is suitable for the electrochemical deposition owing to the waiting time of material diffusion into the porous layer. For the flat substrate, therefore, the application of a constant voltage can be available, but it depends on the diffusion of the reactant in the electrolyte. The electrolyte solvent is basically water. Although the layers by electrochemical deposition are basically metals, nonmetal materials (metal oxides, metal sulfides, and selenium) can also be deposited by controlling the deposition condition (Figure 23).

CONCLUSIONS

As can be seen, the progress of human beings about printed solar cells has been marvellous in the last two

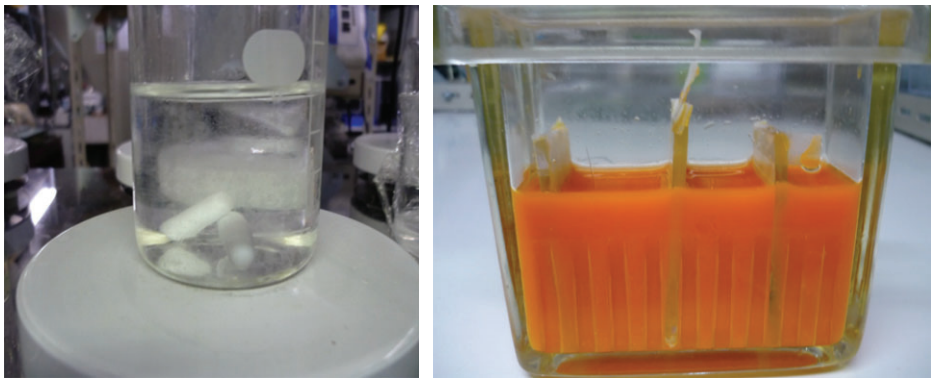

FIGURE 22 | Photographs of solutions for chemical bath deposition of Sb_2S_3 on porous TiO_2 layer; left: before deposition (transparent); right: after deposition (orange).[74,77]

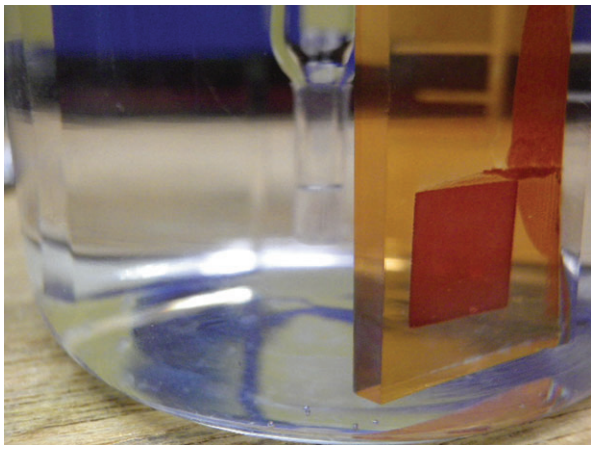

FIGURE 23 | Photograph of electrochemical deposition of selenium on porous TiO_2 layer.[123]

decades. Finding the first emergence of silicon solar cells, scientists found that they needed cost-effective solar cells, which could be achieved by printing methods, and struggled to give their contribution to each subject. Concerning DSCs, in 1976, Matsumura investigated liquid-state DSCs using porous ZnO with the efficiency of 1%. Later, in 1991, Grätzel improved the efficiency to 7% using a nanocrystalline-TiO_2 electrode and ruthenium dye attached to the TiO_2 electrode. Now, the 15% conversion efficiency of solid-state solar cells using porous oxide electrodes has been achieved. Concerning OPV, in 1986, Tang investigated organic p-n junction thin-film solar cells using the vacuum deposition method. The efficiency of the first stage was only 1%. Now, the efficiency of organic thin-film solar cells has risen up to 12%. Although the organic solar cells have been very weak against water and oxygen, Takahashi found a new combination with which the organic solar cells can survive without encapsulations.

The high-conversion efficiency compound (CIGS) solar cells have been fabricated by vacuum deposition methods. At the same time, new non-vacuum methods for CIGS solar cells have been investigated. Without indium, CZTS solar cells also emerged as printed solar cells. On the other hand, the back contact of molybdenum and the front contact of Al-doped ZnO (AZO) have been fabricated by the vacuum deposition process for substrate compound solar cells. If the process can be performed only by sputtering, the full-dry-deposition processing would also be very promising. Such progress has just emerged from the collaborations between AIST (Niki group, Japan) and Canon Anelva Co. Ltd. (Japan).[132] Possibly, the present CIGS solar cells by vacuum deposition will also be even cheaper as cost-effective solar cells.

In conclusion, a lot of new solar cells (DSC, CIGS, CZTS, OPV, etc.) with new processing methods and new materials are emerging as energy resources. Efforts should be continued for the future benefit.

REFERENCES

1. Mendonça M. *Feed-in Tariffs (Accelerating the Deployment of Renewable Energy)*. London: Earthscan; 2007, 91.
2. Knoll B, Kreutzmann A. Prior to sanctions. *Photon Int* 2013, 6:48–55.
3. New Energy and Industrial Technology Development Organization (NEDO). Overview of "PV Roadmap Toward 2030+ (PV2030+)." New Energy and Industrial Technology Development Organization (NEDO), Japan. Available at:

http://www.nedo.go.jp/library/pv2030_index.html. (Accessed February 3, 2014).

4. Krause MB. Technological puzzle. *Photon Int* 2013, 2:60–63.
5. Chirila A, Reinhard P, Pianezzi F, Bloesch P, Uhl AR, Fella C, Kranz L, Keller D, Gretener C, Hagendorfer H, Jaeger D, Erni R, Nishiwaki S, Buecheler S, Tiwari AN. Potassium-induced surface modification of Cu(In,Ga)Se2 thin films for high-efficiency solar cells. *Nature Mater* 2013, 12:1107–1111.
6. Tsubomura H, Matsumura M, Nomura Y, Amamiya T. Dye sensitised zinc oxide: aqueous electrolyte: platinum photocell. *Nature* 1976, 261:402–403.
7. O'Regan B, Grätzel M. A low-cost, high-efficiency solar cell based on dye-sensitized colloidal TiO_2 films. *Nature* 1991, 353:737–740.
8. Nazzerruddin MK, Kay A, Podicio I, Humphy-Baker R, Müller E, Liska P, Vlachopoulos N, Grätzel M. Conversion of light to electricity by cis-X_2 bis(2,2′-bipyridyl-4,4′-dicarboxylate)ruthenium(II) charge-transfer sensitizers ($X = Cl^-, Br^-, I^-, CN^-$, and SCN^-) on nanocrystalline titanium dioxide electrodes. *J Am Chem Soc* 1993, 115:6382–6390.
9. Ito S, Murakami TN, Comte P, Liska P, Grätzel C, Nazeeruddin MK, Grätzel M. Fabrication of thin film dye sensitized solar cells with solar to electric power conversion efficiency over 10%. *Thin Solid Films* 2008, 516:4613–4619.
10. Nazeeruddin MK, De Angelis F, Fantacci S, Selloni A, Viscardi G, Liska P, Ito S, Takeru B, Grätzel M. Combined experimental and DFT-TDDFT computational study of photoelectrochemical cell ruthenium sensitizers. *J Am Chem Soc* 2005, 127:16835–16847.
11. Yella A, Lee HW, Tsao HN, Yi C, Chandiran AK, Nazeeruddin MK, Diau EWG, Yeh CY, Zakeeruddin SM, Grätzel M. Porphyrin-sensitized solar cells with cobalt (II/III)-based redox electrolyte exceed 12 percent efficiency. *Science* 2011, 334:629–634.
12. Han L, Islam A, Chen H, Malapaka C, Chiranjeevi B, Zhang S, Yang X, Yanagida M. High-efficiency dye-sensitized solar cell with a novel co-adsorbent. *Energy Environ Sci* 2012, 5:6057–6060.
13. Grätzel M. Nanostructured photosystems for the generation of electricity from sunlight. In: *EMRS Spring Meeting*, Strasbourg, France, 2013, II 2.
14. Kojima A, Teshima K, Shirai Y, Miyasaka T. Organometal halide perovskites as visible-light sensitizers for photovoltaic cells. *J Am Chem Soc* 2009, 131: 6050–6051.
15. Kopidakis N, Schiff EA, Park NG, van de Lagemaat J, Frank AJ. Ambipolar diffusion of photocarriers in electrolyte-filled, nanoporous TiO_2. *J Phys Chem B* 2000, 104:3930–3936.
16. Kambe S, Nakade S, Kitamura T, Wada Y, Yanagida S. Influence of the electrolytes on electron transport in mesoporous TiO_2-electrolyte systems. *J Phys Chem B* 2002, 106:2967–2972.
17. Kopidakis N, Neale NR, Zhu K, van de Lagemaat J, Frank AJ. Spatial location of transport-limiting traps in TiO_2 nanoparticle films in dye-sensitized solar cells. *Appl Phys Lett* 2005, 87:202106.
18. Zhu K, Kopidakis N, Neale NR, van de Lagemaat J, Frank AJ. Influence of surface area on charge transport and recombination in dye-sensitized TiO_2 solar cells. *J Phys Chem B* 2006, 110:25174–25180.
19. Würfel U, Peters M, Hinsch A. Detailed experimental and theoretical investigation of the electron transport in a dye solar cell by means of a three-electrode configuration. *J Phys Chem C* 2008, 112:1711–1720.
20. Wang P, Klein C, Humphry-Baker R, Zakeeruddin SM, Grätzel M. Stable >8% efficient nanocrystalline dye-sensitized solar cell based on an electrolyte of low volatility. *Appl Phys Lett* 2005, 86:123508.
21. The Nikkan Kogyo Shimbun, May 22, 2012. Available at: http://www.nikkan.co.jp/news/nkx0520120522cbaj.html. (Accessed September 4, 2013).
22. Kumara GRA, Kaneko S, Konno A, Okuya M, Tennakone K. Dye-sensitized solar cells with an extremely thin liquid film as the redox electron mediator. *Chem Lett* 2005, 34:572–573.
23. Hagen J, Schaffrath W, Otschik P, Fink R, Bacher A, Schmidt HW, Haarer D. Novel hybrid solar cells consisting of inorganic nanoparticles and an organic hole transport material. *Synth Met* 1997, 89:215–220.
24. Bach U, Lupo D, Comte P, Moser JE, Weissörtel F, Salbeck J, Spreitzer H, Grätzel M. Solid-state dye-sensitized mesoporous TiO_2 solar cells with high photon-to-electron conversion efficiencies. *Nature* 1998, 395:583–585.
25. Krüger J, Plass R, Grätzel M, Matthieu HJ. Improvement of the photovoltaic performance of solid-state dye-sensitized device by silver complexation of the sensitizer cis-bis(4,4′-dicarboxy-2,2′bipyridine)-bis(isothiocyanato) ruthenium(II). *Appl Phys Lett* 2002, 81:367–369.
26. Schmidt-Mende L, Zakeeruddin SM, Grätzel M. Efficiency improvement in solid-state-dye-sensitized photovoltaics with an amphiphilic Ruthenium-dye. *Appl Phys Lett* 2005, 86:013504.
27. Schmidt-Mende L, Bach U, Humphry-Baker R, Horiuchi T, Miura H, Ito S, Uchida S, Graetzel M. Organic dye for highly efficient solid-state dye-sensitized solar cells. *Adv Mater* 2005, 17:813–815.
28. Snaith HJ, Moule AJ, Klein C, Meerholz K, Friend RH, Grätzel M. Efficiency enhancements in solid-state hybrid solar cells via reduced charge recombination and increased light capture. *Nano Lett* 2007, 7:3372–3376.
29. Moon SJ, Itzhaik Y, Yum JH, Zakeeruddin SM, Hodes G, Grätzel M. Sb_2S_3-based mesoscopic solar cell using

an organic hole conductor. *J Phys Chem Lett* 2010, 1:1524–1527.

30. Burschka J, Dualeh A, Kessler F, Barano E, Cevey-Ha NL, Yi C, Nazeeruddin MK, Grätzel M. Tris(2-(1H-pyrazol-1-yl)pyridine)cobalt(III) as p-type dopant for organic semiconductors and its application in highly efficient solid-state dye-sensitized solar cells. *J Am Chem Soc* 2011, 133:18042–18045.
31. Kim HS, Lee CR, Im JH, Lee KB, Moehl T, Marchioro A, Moon SJ, Humphry-Baker R, Yum JH, Moser JE, et al. Lead iodide perovskite sensitized all-solid-state submicron thin film mesoscopic solar cell with efficiency exceeding 9%. *Sci Rep* 2012, 2:591.
32. Lee MM, Teuscher J, Miyasaka T, Murakami TN, Snaith HJ. Efficient hybrid solar cells based on meso-superstructured organometal halide perovskites. *Science* 2012, 338:643–647.
33. Ball JM, Lee MM, Hey A, Snaith HJ. Low-temperature processed meso-superstructured to thin-film perovskite solar cells. *Energy Environ Sci* 2013, 6:1739–1743.
34. Burschka J, Pellet N, Moon S, Humphry-Baker R, Gao P, Nazeeruddin MK, Grätzel M. Sequential deposition as a route to high-performance perovskite-sensitized solar cells. *Nature* 2013, 499:316–319.
35. Liu M, Johnston MB, Snaith HJ. Efficient planar heterojunction perovskite solar cells by vapour deposition. *Nature* 2013, 501: 395–398.
36. Murakoshi K, Kogure R, Wada Y, Yanagida S. Solid state dye-sensitized TiO_2 solar cell with polypyrrole as hole transport layer. *Chem Lett* 1997:471–472.
37. Thelakkat M, Hagen J, Haarer D, Schmidt HW. Poly(triarylamine)s- synthesis and application in electroluminescent devices and photovoltaics. *Synth Met* 1999, 102:1125–1128.
38. Spiekermammn S, Smestad G, Kowalik J, Tolbert LM, Grätzel M. Poly(4-undecyl-2,2′-bithiophene) as a hole conductor in solid stage dye sensitized titanium dioxide solar cells. *Synth Met* 2001, 121:1603–1604.
39. Kitamura T, Maitani M, Matsuda M, Wada Y, Yanagida S. Improved solid-state dye solar cells with polypyrrole using a carbon-based counter electrode. *Chem Lett* 2001, 30:1054–1055.
40. Gebeyehu D, Brabec CJ, Sariciftci NS. Solid-state organicyinorganic hybrid solar cells based on conjugated polymers and dye-sensitized TiO_2 electrodes. *Thin Solid Films* 2002, 403–404:271–274.
41. Saito Y, Fukuri N, Senadeera R, Kitamura T, Wada Y, Yanagida S. Solid state dye sensitized solar cells using in situ polymerized PEDOTs as hole conductor. *Electrochem Commun* 2004, 6:71–74.
42. Wang Y, Yang K, Kim SC, Nagarajan R, Samuelson LA, Kumar J. In situ polymerized carboxylated diacetylene as a hole conductor in solid-state dye-sensitized solar cells. *Chem Mater* 2006, 18: 4215–4217.
43. Fukuri N, Masaki N, Kitamura T, Wada Y, Yanagida S. Electron transport analysis for improvement of solid-state dye-sensitized solar cells using poly(3,4-ethylenedioxythiophene) as hole conductors. *J Phys Chem B* 2006, 110:25251–25258.
44. Mozer AJ, Wada Y, Jiang KJ, Masaki N, Yanagida S, Mori SN. Efficient dye-sensitized solar cells based on a 2-thiophen-2-yl-vinylconjugated ruthenium photosensitizer and a conjugated polymer hole conductor. *Appl Phys Lett* 2006, 89:043509.
45. Haeldermans I, Truijen I, Vandewal K, Moons W, Van Bael MK, D'Haen J, Manca JV, Mullens J. Water based preparation method for 'green' solid-state polythiophene solar cells. *Thin Solid Films* 2008, 516:7245–7250.
46. Xia J, Masaki N, Lira-Cantu M, Kim Y, Jiang K, Yanagida S. Influence of doped anions on poly(3,4-ethylenedioxythiophene) as hole conductors for iodine-free solid-state dye-sensitized solar cells. *J Am Chem Soc* 2008, 130:1258–1263.
47. Liu X, Zhang W, Uchida S, Cai L, Liu B, Ramakrishna S. An efficient organic-dye-sensitized solar cell with in situ polymerized poly(3,4-ethylenedioxythiophene) as a hole-transporting material. *Adv Mater* 2010, 22:E150–E155.
48. Chang JA, Rhee JH, Im SH, Lee YH, Kim HJ, Seok SI, Nazeeruddin MK, Grätzel M. High-performance nanostructured inorganic-organic heterojunction solar cells. *Nano Lett* 2010, 10:2609–2612.
49. Im SH, Lim CS, Chang JA, Lee YH, Maiti N, Kim HJ, Nazeeruddin MK, Grätzel M, Seok SI. Toward interaction of sensitizer and functional moieties in hole-transporting materials for efficient semiconductor-sensitized solar cells. *Nano Lett* 2011, 11:4789–4793.
50. Yang L, Cappel UB, Unger EL, Karlsson M, Karlsson KM, Gabrielsson E, Sun L, Boschloo G, Hagfeldt A, Johansson EMJ. Comparing spiro-OMeTAD and P3HT hole conductors in efficient solid state dye-sensitized solar cells. *Phys Chem Chem Phys* 2012, 14:779–789.
51. Noh JH, Im SH, Heo JH, Mandal TN, Seok SI. Chemical management for colorful, efficient, and stable inorganic-organic hybrid nanostructured solar cells. *Nano Lett* 2013, 13:1764–1769.
52. Heo JH, Im SH, Noh JH, Mandal TN, Lim CS, Chang JA, Lee YH, Kim HJ, Sarkar A, Nazeeruddin MK, et al. Efficient inorganic–organic hybrid heterojunction solar cells containing perovskite compound and polymeric hole conductors. *Nat Photon* 2013, 7:486–491.
53. Liu Q, Li C, Jiang K, Song Y, Pei J. A high-efficiency solid-state dye-sensitized solar cell with P3HT polymer as a hole conductor and an assistant sensitizer. *Particuology*. In press.
54. Tennakone K, Kumara GRRA, Kumarasinghe AR, Wijayantha KGU, Sirimanne PM. A dye-sensitized

nano-porous solid-state photovoltaic cell. *Semicond Sci Technol* 1995, 10:1689.

55. O'Regan B, Schwatrz DT. Efficient dye-sensitized charge separation in a wide-band-gap p-n heterojunction. *J Appl Phys* 1996, 80:4749–4754.
56. Tennakone K, Kumara GRRA, Wijayantha KGU, Kottegoda IRM, Perera VPS, Aponsu GMLP. A nanoporous solid-state photovoltaic cell sensitized with copper chlorophyllin. *J Photochem Photobiol A: Chem* 1997, 108:175–177.
57. O'Regan B, Schwatrz DT. Illumination of the dye-sensitized heterojunction TiO_2/RuLL'NCS/CuSCN: initiation and potential mechanisms. *Chem Mater* 1998, 10:1501–1509.
58. Tennakone K, Kumara GRRA, Kottegoda IRM, Perera VPS, Weerasundara PSRS. Sensitization of nanoporous films of TiO_2 with santalin (red sandalwood pigment) and construction of dye-sensitized solid-state photovoltaic cells. *J Photochem Photobiol A: Chem* 1998, 117:137–142.
59. Tennakone K, Kumara GRRA, Kottegoda IRM, Wijayantha KGU, Perera VPS. A solid-state photovoltaic cell sensitized with a ruthenium bipyridyl complex. *J Phys D Appl Phys* 1998, 31:1492–1496.
60. Tennakone K, Kumara GRRA, Kottegoda IRM, Perera VPS, Aponsu GMLP. Nanoporous n-TiO_2/selenium/p-CuCNS photovoltaic cell. *J Phys D Appl Phys* 1998, 31:2326–2330.
61. Tennakone K, Perera VPS, Kottegoda IRM, Kumara GRRA. Dye-sensitized solid state photovoltaic cell based on composite zinc oxide/tin (IV) oxide films. *J Phys D Appl Phys* 1999, 32:374–379.
62. O'Regan B, Schwartz DT, Zakeeruddin SM, Grätzel M. Electrodeposited nanocomposite n-p heterojunctions for solid-state dye-sensitized photovoltaics. *Adv Mater* 2000, 12:1263–1267.
63. Tennakone K, Senadeera GKR, De Silva DBRA, Kottegoda IRM. Highly stable dye-sensitized solid-state solar cell with the semiconductor 4CuBr 3S$(C_4H_9)_2$ as the hole collector. *Appl Phys Lett* 2000, 77:2367–2369.
64. Kumara GRRA, Konno A, Senadeera GKR, Jayaweerab PVV, De Silvab DBRA, Tennakone K. Dye-sensitized solar cell with the hole collector p-CuSCN deposited from a solution in n-propyl sulphide. *Solar Energy Mater Solar Cells* 2001, 69:195–199.
65. O'Regan B, Lenzmann F, Muis R, Wienke J. A solid-state dye-sensitized solar cell fabricated with pressure-treated P25-TiO_2 and CuSCN: analysis of pore filling and IV characteristics. *Chem Mater* 2002, 14:5023–5029.
66. Kumara GRA, Okuya M, Murakami K, Kaneko S, Jayaweera VV, Tennakone K. Dye-sensitized solid-state solar cells made from magnesium oxide-coated nanocrystalline titanium dioxide films: enhancement of the efficiency. *J Photochem Photobiol A: Chem* 2004, 164:183–185.
67. Perera VPS, Senevirathna MKI, Pitigala PKDDP, Tennakone K. Doping CuSCN films for enhancement of conductivity: application in dye-sensitized solid-state solar cells. *Solar Energy Mater Solar Cells* 2005, 86:443–450.
68. Lévy-Clément C, Tena-Zaera R, Ryan MA, Katty A, Hodes G. CdSe-sensitized p-CuSCN/nanowire n-ZnO heterojunctions. *Adv Mater* 2005, 17:1512–1515.
69. Larramona G, Choné C, Jacob A, Sakakura D, Delatouche B, Péré D, Cieren X, Nagino M, Bayón R. Nanostructured photovoltaic cell of the type titanium dioxide, cadmium sulfide thin coating, and copper thiocyanate showing high quantum efficiency. *Chem Mater* 2006, 18:1688–1696.
70. Konno A, Rajanya G, Kumara A, Kaneko S, Onwona-Agyeman B, Tennakone K. Solid-state solar cells sensitized with indoline dye. *Chem Lett* 2007, 36:716–717.
71. Dittrich T, Kieven D, Tornow J, Schwarzburg K, Lux-Steiner MC. Influence of the local absorber layer thickness on the performance of ZnO nanorod solar cells. *Phys Stat Sol RRL* 2008, 2:172–174.
72. Itzhaik Y, Niitsoo O, Page M, Hodes G. Sb_2S_3-sensitized nanoporous TiO_2 solar cells. *J Phys Chem C* 2009, 113:4254–4256.
73. Nezu S, Larramona G, Choné C, Jacob A, Delatouche B, Péré D, Moisan C. Light soaking and gas effect on nanocrystalline TiO_2/Sb_2S_3/CuSCN photovoltaic cells following extremely thin absorber concept. *J Phys Chem C* 2010, 114:6854–6859.
74. Tsujimoto K, Nguyen DC, Ito S, Nishino H, Matsuyoshi H, Konno A, Kumara GRRA, Tennakone K. TiO_2 surface treatment effects by Mg^{2+}, Ba^{2+}, and Al^{3+} on Sb_2S_3 extremely thin absorber solar cells. *J Phys Chem C* 2012, 116:13465–13471.
75. Moribe S, Takeichi A, Seki J, Kato N, Higuchi K, Ueyama K, Mizumoto K, Toyoda T. Improved performance of solid-state dye-sensitized solar cells with CuI: structure control of porous TiO_2 films. *Appl Phys Express* 2012, 5:112302.
76. Premalal EVA, Dematage N, Kumara GRRA, Rajapakse RMG, Shimomura M, Murakami K, Konno A. Preparation of structurally modified, conductivity enhanced-p-CuSCN and its application in dye-sensitized solid-state solar cells. *J Power Sources* 2012, 203:288–296.
77. Ito S, Tsujimoto K, Nguyen DC, Manabe K, Nishino H. Doping effects in Sb_2S_3 absorber for full-inorganic printed solar cells with 5.7% conversion efficiency. *Int J Hydrogen Energy* 2013, 38:16749–16754.
78. Ito S. Full-inorganic all-solid printed solar cells. In: *EMRS Spring Meeting*, Strasbourg, France, 2013, XIV 1.

79. Savadogo O, Mandal KC. Studies on new chemically deposited photoconducting antimony trisulphide thin films. *Solar Energy Mater Solar Cells* 1992, 26:117–136.

80. Nair MTS, Peña Y, Campos J, García VM, Nair PK. Chemically deposited Sb_2S_3 and Sb_2S_3-CuS thin films. *J Electrochem Soc* 1998, 145:2113–2120.

81. Jackson P, Hariskos D, Lotter E, Paetel S, Wuerz R, Menner R, Wischmann W, Powalla M. New world record efficiency for Cu(In,Ga)Se_2 thin-film solar cells beyond 20%. *Prog Photovolt: Res Appl* 2011, 19:894–897.

82. Kobayashi T, Yamaguchi H, Nakada T. Effects of combined heat and light soaking on device performance of Cu(In,Ga)Se_2 solar cells with ZnS(O,OH) buffer layer. *Prog Photovolt: Res Appl* 2014, 22:115–121.

83. Katagiri H, Sasaguchi N, Hando S, Hoshino S, Ohashi J, Yokota T. Preparation films by and evaluation of Cu_2ZnSnS_4 thin sulfurization of E-B evaporated precursors. *Solar Energy Mater Solar Cells* 1997, 49:407–414.

84. Katagiri H, Jimbo K, Maw WS, Oishi K, Yamazaki M, Araki H, Takeuchi A. Development of CZTS-based thin film solar cells. *Thin Solid Films* 2009, 517:2455–2460.

85. Repins I, Beall C, Vora N, DeHart C, Kuciauskas D, Dippo P, To B, Mann J, Hsu WC, Goodrich A, et al. Co-evaporated $Cu_2ZnSnSe_4$ films and devices. *Solar Energy Mater Solar Cells* 2012, 101:154–159.

86. Todorov TK, Tang J, Bag S, Gunawan O, Gokmen T, Zhu Y, Mitzi DB. Beyond 11% efficiency: characteristics of state-of-the-art $Cu_2ZnSn(S,Se)_4$ solar cells. *Adv Energy Mater* 2013, 3:34–38.

87. Todorov TK, Gunawan O, Gokmen T, Mitzi DB. Solution-processed Cu(In,Ga)$(S,Se)_2$ absorber yielding a 15.2% efficient solar cell. *Prog Photovolt: Res Appl* 2013, 21:82–87.

88. Guo Q, Ford GM, Agrawal R, Hillhouse HW. Ink formulation and low-temperature incorporation of sodium to yield 12% efficient Cu(In,Ga)$(S,Se)_2$ solar cells from sulfide nanocrystal inks. *Prog Photovolt: Res Appl* 2013, 21:64–71.

89. Guo Q, Ford GM, Yang WC, Hages CJ, Hillhouse HW, Agrawal R. Enhancing the performance of CZTSSe solar cells with Ge alloying. *Solar Energy Mater Solar Cells* 2012, 105:132–136.

90. Nguyen DC, Fukatsu K, Tanimoto K, Ikada S, Matsumura M, Ito S. The effect of annealing temperature and KCN etching on microstructural and photovoltaic properties of Cu(In,Ga)$(S,Se)_2$ solar cells using nanoparticles. *Int J Photoenergy* 2013, 2013:416245.

91. Park SJ, Cho JW, Lee JK, Shin K, Kim JH, Min BK. Solution processed high band-gap $CuInGaS_2$ thin film for solar cell applications. *Prog Photovolt: Res Appl* 2014, 22:122–128.

92. Pattantyus-Abraham AG, Kramer IJ, Barkhouse AR, Wang X, Konstantatos G, Debnath R, Levina L, Raabe I, Nazeeruddin MK, Grätzel M, et al. Depleted-heterojunction colloidal quantum dot solar cells. *ACS Nano* 2010, 4:3374–3380.

93. Tang J, Kemp KW, Hoogland S, Jeong KS, Liu H, Levina L, Furukawa M, Wang X, Debnath R, Cha D, et al. Colloidal-quantum-dot photovoltaics using atomic-ligand passivation. *Nat Mater* 2011, 10:765–771.

94. Jianbo G, Craig LP, Joseph ML, Hanna MC, Chen HYO, Semonin E, Nozik AJ, Ellingson RJ, Beard MC. n-Type transition metal oxide as a hole extraction layer in PbS quantum dot solar cells. *Nano Lett* 2011, 11:3263–3266.

95. Etgar L, Zhang W, Gabriel S, Hickey SG, Nazeeruddin MK, Eychmüller A, Liu B, Grätzel M. High efficiency quantum dot heterojunction solar cell using anatase (001) TiO_2 nanosheets. *Adv Mater* 2012, 24:2202–2206.

96. Etgar L, Gao P, Xue Z, Peng Q, Chandiran AK, Liu B, Nazeeruddin MK, Grätzel M. Mesoscopic $CH_3NH_3PbI_3/TiO_2$ heterojunction solar cells. *J Am Chem Soc* 2012, 134:17396–17399.

97. Wada T, Kinoshita H, Kawata S. Preparation of chalcopyrite-type $CuInSe_2$ by non-heating process. *Thin Solid Films* 2003, 431–432:11–15.

98. Wada T, Matsuo Y, Nomura S, Nakamura Y, Miyamura A, Chiba Y, Yamada A, Konagai M. Fabrication of Cu(In,Ga)Se_2 thin films by a combination of mechanochemical and screen-printing/sintering processes. *Phys Stat Sol (a)* 2006, 203: 2593–2597.

99. Nguyen DC, Ito S, Inoue M, Yusa S. Superstrate $CuInSe_2$-printed solar cells on In_2S_3/TiO_2/FTO/glass plates. *Energy Sci Technol* 2012, 3:1–8.

100. Nguyen DC, Ito S. Cu_2Te solar cells fabricated by printing. *Int J Nanotechnol* 2013, 10:269–278.

101. Nguyen DC, Ito S. Narrow band gap $AgInTe_2$ solar cells fabricated by printing method. *Energy Sci Technol* 2012, 4:1–5.

102. Goossens A, Hofhuis J. Spray-deposited $CuInS_2$ solar cells. *Nanotechnology* 2008, 19:424018.

103. John TT, Mathew M, Sudha Kartha C, Vijayakumar KP, Abe T, Kashiwaba Y. $CuInS_2/In_2S_3$ thin film solar cell using spray pyrolysis technique having 9.5% efficiency. *Solar Energy Mater Solar Cells* 2005, 89:27–36.

104. Valdés MH, Berruet M, Goossens A, Vázquez M. Spray deposition of $CuInS_2$ on electrodeposited ZnO for low-cost solar cells. *Surf Coat Technol* 2010, 204:3995–4000.

105. Cherian AS, Abe T, Kashiwaba Y, Sudha Kartha C, Vijayakumar KP. $CuInS_2/In_2S_3$ cells using a cost-effective technique: significance of precursor ratios on cell parameters. *Energy Procedia* 2012, 15: 283–290.

106. Ryo T, Nguyen DC, Nakagiri M, Toyoda N, Matsuyoshi H, Ito S. Characterization of superstrate type $CuInS_2$ solar cells deposited by spray pyrolysis method. *Thin Solid Films* 2011, 519:7184–7188.

107. Nguyen DC, Mikami Y, Tsujimoto K, Ryo T, Ito S. Spray-pyrolyzed three-dimensional $CuInS_2$ solar cells on nanocrystalline-titania electrodes with chemical-bath-deposited Inx(OH)ySz buffer layers. *Jpn J Appl Phys* 2012, 51:10NC23.

108. Hanaro N, Nguyen DC, Ito S. $CuInS_2$ superstrate solar cells with ZnO compact layer fabricated by totally non-vacuum methods. *J Adv Oxid Technol* 2013, 16:102–106.

109. Krunks M, Kärber E, Katerski A, Otto K, Oja Acik I, Dedova T, Mere A. Extremely thin absorber layer solar cells on zinc oxide nanorods by chemical spray. *Solar Energy Mater Solar Cells* 2010, 94: 1191–1195.

110. Nguyen DC, Ryo T, Lombez L, Ito S. Effect of Na and Ti-doping on photovoltaic properties of $CuInS_2$ solar cells. *Int J Nanotechnol* 2013, 10:279–287.

111. Ito S, Ryo T. Segregation of Cu-In-S elements in the spray-pyrolysis-deposited layer of CIS solar cells. *Adv Mater Sci Eng* 2012, 2012:136092.

112. Kim SY, Kim JH. Effect of selenization on sprayed $Cu_2ZnSnSe_4$ thin film solar cell. *Thin Solid Films* 2013, 547:178–180.

113. Rajeshmon VG, Poornima N, Sudha Kartha C, Vijayakumar KP. Modification of the optoelectronic properties of sprayed In_2S_3 thin films by indium diffusion for application as buffer layer in CZTS based solar cell. *J Alloys Compd* 2013, 553:239–244.

114. Kitagawa N, Ito S, Nguyen DC, Nishino H. Copper zinc sulfur compound solar cells fabricated by spray pyrolysis deposition for solar cells. *Nat Resour* 2013, 4:142–145.

115. Nguyen DC, Takehara K, Ryo T, Ito S. Back contact materials for superstrate $CuInS_2$ solar cells. *Energy Procedia* 2011, 10:49–54.

116. Lincot D, Guillemoles JF, Taunier S, Guimard D, Sicx-Kurdi J, Chaumont A, Roussel O, Ramdani O, Hubert C, Fauvarque JP, et al. Chalcopyrite thin film solar cells by electrodeposition. *Solar Energy* 2004, 77:725–737.

117. Lee SM, Ikeda S, Otsuka Y, Septina W, Harada T, Matsumura M. Homogeneous electrochemical deposition of in on a Cu-covered Mo substrate for fabrication of efficient solar cells with a $CuInS_2$ photoabsorber. *Electrochim Acta* 2012, 79: 189–196.

118. Duchatelet A, Savidand G, Vannier RN, Chassaing E, Lincot D. A new deposition process for $Cu(In,Ga)(S,Se)_2$ solar cells by one-step electrodeposition of mixed oxide precursor films and thermochemical reduction. *J Renewable Sustainable Energy* 2013, 5:011203.

119. Pawar SM, Pawar BS, Gurav KV, Bae DW, Kwon SH, Kolekar SS, Kim JH. Fabrication of Cu_2ZnSnS_4 thin film solar cell using single step electrodeposition method. *Jpn J Appl Phys* 2012, 51:10NC27.

120. Scragg JJ, Berg DM, Dale PJ. A 3.2% efficient Kesterite device from electrodeposited stacked elemental layers. *J Electroanal Chem* 2010, 646:52–59.

121. Ennaoui A, Lux-Steiner M, Weber A, Abou-Ras D, Kötschau I, Schock HW, Schurr R, Hölzing A, Jost S, Hock R, et al. Cu_2ZnSnS_4 thin film solar cells from electroplated precursors: novel low-cost perspective. *Thin Solid Films* 2009, 517:2511–2514.

122. Guo L, Zhu Y, Gunawan O, Gokmen T, Deline VR, Ahmed S, Romankiw LT, Deligianni H. Electrodeposited $Cu_2ZnSnSe_4$ thin film solar cell with 7% power conversion efficiency. *Prog Photovolt: Res Appl* 2014, 22:58–68.

123. Nguyen DC, Tanaka S, Nishino H, Manabe K, Ito S. 3-D solar cells by electrochemical-deposited Se layer as extremely-thin absorber and hole conducting layer on nanocrystalline TiO_2 electrode. *Nanoscale Res Lett* 2013, 8:8.

124. Tang CW. Two-layer organic photovoltaic cell. *Appl Phys Lett* 1986, 48:183–185.

125. Hiramoto M, Fujiwara H, Yokoyama M. Three-layered organic solar cell with a photoactive interlayer of codeposited pigments. *Appl Phys Lett* 1991, 58:1062–1064.

126. Sariciftci NS, Smilowitz L, Heeger AJ, Wudl F. Photoinduced electron transfer from a conducting polymer to buckminsterfullerene. *Science* 1992, 258:1474–1476.

127. Yu G, Gao J, Hummelen JC, Wudl F, Heeger AJ. Polymer photovoltaic cells: enhanced efficiencies via a network of internal donor-acceptor heterojunctions. *Science* 1995, 270:1789–1791.

128. Kim JY, Lee K, Coates NE, Moses D, Nguyen TQ, Dante M, Heeger AJ. Efficient tandem polymer solar cells fabricated by all-solution processing. *Science* 2007, 317:222–225.

129. He ZC, Zhong CM, Su SJ, Xu M, Wu HB, Cao Y. Enhanced power-conversion efficiency in polymer solar cells using an inverted device structure. *Nat Photon* 2012, 6:591–595.

130. You JB, Dou LT, Yoshimura K, Kato T, Ohya K, Moriarty T, Emery K, Chen CC, Gao J, Li G, et al. A polymer tandem solar cell with 10.6% power conversion efficiency. *Nat Commun* 2013, 4: 1446.

131. Kuwabara T, Sugiyama H, Kuzuba M, Yamaguchi T, Takahashi K. Inverted bulk-heterojunction organic solar cell using chemical bath deposited titanium oxide as electron collection layer. *Org Electron* 2010, 11:1136–1140.

132. Sato M, Watabe O, Nakagawa T, Shibata H, Niki S. Efficiency improvement of CIGS solar cells using sputter-deposited buffer layer. In: *The 60th Spring Meeting of the Japan Society of Applied Physics*, 2013, 14.5:28a-G4-7.

